Lawrence Berkeley Laboratory
UNIVERSITY OF CALIFORNIA

Materials & Molecular Research Division

MOLECULAR BEAM STUDIES OF THE F + D₂ and F + HD REACTION

D.M. Neumark, A.M. Wodtke, G.N. Robinson,
C.C. Hayden, K. Shobatake, R.K. Sparks,
T.P. Schafer, and Y.T. Lee

August 1984

DISCLAIMER
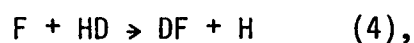
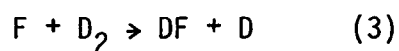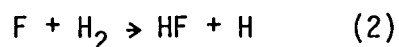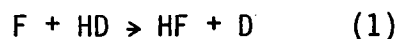# MOLECULAR BEAM STUDIES OF THE F + D$_2$ and F + HD REACTION

D. M. Neumark, A. M. Wodtke, G. N. Robinson, C. C. Hayden,
K. Shobatake, R. K. Sparks, T. P. Schafer, and Y. T. Lee

Materials and Molecular Research Division, Lawrence Berkeley Laboratory
and Department of Chemistry, University of California
Berkeley, California 94720 USA

1. Introduction

The previous paper described a high resolution crossed molecular beam investigation of the F + H_2 reaction in which center-of-mass angular and kinetic energy distributions were determined for each HF product vibrational state. This paper discusses similar work on the F + D_2 and F + HD reactions. The purpose of these studies was to observe trends in the series,

$$F + HD \rightarrow HF + D \qquad (1)$$

$$F + H_2 \rightarrow HF + H \qquad (2)$$

$$F + D_2 \rightarrow DF + D \qquad (3)$$

$$F + HD \rightarrow DF + H \qquad (4),$$

in order to obtain a global perspective on the dynamics of this fundamental set of reactions. In particular, we sought further support for our explanation of the F + H_2 results in terms of dynamical resonances by determining the effect of isotopic substitution on the product angular distributions.

Previous experimental and theoretical investigations have examined features of these reactions that are sensitive to isotopic substitution. A consistent set of absolute and relative rate constants has been determined in a series of kinetic studies [1-5]. Product energy distributions have been obtained using chemical laser [6] and infrared chemiluminescence [7,8] techniques and were also investigated in classical trajectory studies on model potential energy surfaces [9-11]. The key experimental findings are as follows [8]: (i) all four reactions produce highly inverted product vibrational distributions; (ii) the HF product from reactions (1) and (2) is primarily formed in v = 1 - 3

with the maximum population in v = 2, whereas most of the DF population
from (3) and (4) is in v = 2 - 4 with the maximum population in v = 3.
While the DF vibrational distributions from (3) and (4) are similar,
the HF (v = 3) population from (1) is substantially lower than from
(2); (iii) finally, the fraction of available energy in product rota-
tion, $<f_R>$, decreases progressively from (1) to (4).

Most of the trends are readily explained by the different reac-
tion energetics resulting from the differing zero-point energies and
vibrational energy spacings as shown in fig. 1 [12], and by the re-
sults of classical trajectory calculations. The vibrational popula-
tion distributions are reasonable considering the similar energetics
for producing vibrationally excited HF and DF. The DF (v = 4) and
DF (v = 3) states are at similar energies relative to D_2 (v = 0) as
the HF (v = 3) and HF (v = 2) states are to H_2 (v = 0). The re-
action to form HF (v = 3) from HD is 1.3 kcal/mole endothermic whereas
from H_2 it is only 0.5 kcal/mole endothermic. Thus one would expect
HF (v = 3) from (1) to be suppressed at thermal energies. Classical
trajectory studies have reproduced the trend in product rotational
excitation [11], and this has also been explained using an impulsive
model in which the fraction of product repulsion going into rotation
is determined by a relation between the product masses [13]. The
calculated and experimental values of $<f_v>$, the fraction of avail-
able energy appearing as product vibration, agree reasonably well
although there is some discrepancy between the experiments and tra-
jectory calculations concerning the relative values of $<f_v>$ for HF
and DF from (1) and (4) respectively [2,8,9-11]. The effect of

reactant rotation on the reaction cross section has been studied in
several trajectory calculations [9-11]. The most interesting result,
that the HF/DF branching ratio from F + HD depends strongly on HD
rotation, has still not been experimentally confirmed.

The general agreement between experiment and classical trajectory
calculations breaks down when the reactions are examined in greater
detail. Substantial differences are seen in the product angular
distributions. Molecular beam studies of F + D_2 (14,15) and of
F + H_2 (presented in the previous paper) show predominantly back-
ward scattering of DF and enhanced forward scattering of HF (v = 3).
On the other hand, the angular distributions determined from classical
trajectory studies are dominated by backward scattering for all four
reactions although they show a slight trend towards increased sideways
scattering from (4) to (1) [10,11,17,18]. One is therefore forced to
ask whether the differences in the experimental angular distributions
arise from quantum mechanical reactive scattering effects.

The results of collinear quantal calculations by Schatz et al.[19,20]
of the reaction probability for each product vibrational state vs. col-
lision energy show significant variations in the strength of the dynam-
ical resonances for reactions (1) to (4). The sharp spikes in these
curves are associated with dynamical resonances, and the physical ori-
gin of the resonances was discussed in the previous paper. The curves
for F + D_2 and F + HD $\rightarrow$ DF + H show broad DF features for v = 3 and
v = 4 similar to the v = 2 and v = 3 results from F + H_2 [20]. How-
ever, the sharp resonance in the HF (v = 2) curve is less evident in

the DF ($v = 3$) curve from F + D_2 and disappears in the DF ($v = 3$)
curve from F + HD. The most striking result is the F + HD $\rightarrow$ HF + D
calculation. There is a sharp spike in the HF ($v = 2$) curve near
threshold and virtually no other product at higher collision energies
up to 0.2 ev. The collinear calculations therefore indicate that
reaction (1) is dominated by resonance scattering, and that the
relative contribution of resonant to direct scattering decreases
progressively from (1) to (4).

The potential energy function is the same for all four reactions,
but the kinetic energy terms in the hamiltonian differ for each mass
combination. For a collinear reaction, the mass effects are most
clearly seen in the skewed, mass-weighted coordinate system which
allows the entire reaction to be viewed as the motion of a single
particle in a two-dimensional potential [19]. The skew angle between
the reactant and product valleys is given by $\alpha = \tan^{-1}\left(\dfrac{m_B M}{m_A m_C}\right)^{1/2}$
for A + BC $\rightarrow$ AB + C, where $M = \sum_i m_i$. $\alpha = 37.3°$ for (1), increases pro-
gressively from (1) to (4), and equals 56.7° for (4). The classical
effects of α have been known for some time. At small values of α, col-
linear trajectories are less likely to lead to reaction since the crit-
ical region of the skewed surface becomes more reflective [22]. More
recently, Babamov [23] and Pollak [24] have independently shown that
the vibrationally adiabatic wells and barriers are enhanced at smaller
values of α, and this leads to more pronounced resonance effects.
Thus, while the near absence of direct scattering for F + HD $\rightarrow$ HF + D
is somewhat surprising, the general trends in the quantal collinear
calculations are reasonable in light of the above considerations.

The extension of the collinear calculations to three dimensions was decribed in the previous paper. At collision energies above the $L = 0$ resonance, the angular distribution for the product vibrational state(s) resulting from the decay of the resonance should exhibit increased sideways and forward scattering [25-27]. If the resonance interpretation is correct, then this effect in the angular distributions should be strongest for F + HD $\rightarrow$ HF + D and progressively weaker for reactions (2) – (4). The experimental observation of this trend would therefore support the claim that dynamical resonances play a significant role in the reaction dynamics of F + H_2. The F + HD reaction is especially interesting in this regard, as the HF and DF channels are opposite ends of the 'resonance hierarchy'. Approximate 3-D quantal treatments of F + HD indeed show that the DF product is backward-scattered, whereas the HF product shows strong sideways [28] and, in one calculation, forward scattering [29].

The results of the earlier F + D_2 work and the recent F + H_2 study certainly appear to be consistent with the quantal predictions. The F + D_2 reaction was re-examined with the current high resolution apparatus in order to characterize the product distributions better. The F + HD work reported here is the first crossed molecular beams study of this reaction.

2. Experimental

The apparatus and methodology for these studies were identical to the F + H_2 work described in the previously paper. The detection of DF product was considerably easier than HF product since there was a very low mass 21 background in the detector. The background count

rate was less than 5 Hz with the detector closed off from the main vacuum chamber, and at least some of this was due to field ionization from the 30 kV electrode in our Daly ion counter. There was no contribution from residual rare gas to this mass, and, better still, there was no background problem associated with the F beam as there was when HF was detected, since virtually no F converted to DF inside the F source chambers. As a result, there were no problems in detecting DF reactive signal close to the F beam. The modifications described in the previous paper to lower the mass 20 background were therefore superfluous for the detection of DF.

HD was synthesized in our laboratory by the reaction of D_2O with $LiAlH_4$ dissolved in tetrahydrofuran. The HD was compressed into aluminum storage cylinders at pressures as high as 1500 psi. Its purity was checked by photoionization mass spectroscopy and was estimated to be 98%. Before admitting the HD to the beam source, it was passed through a molecular sieve trap immersed in liquid nitrogen in order to remove atmospheric impurities which might be introduced during the synthesis.

3. Results

Angular distributions of the products from $F + D_2$ and $F + HD$ were taken at several collision energies. The beam conditions for all the scans are displayed in Table 1. The DF LAB angular distributions from $F + D_2$ are shown in figs. 2-4. Θ_{CM} is the angle between the LAB velocity vector for the F beam and the most probable LAB velocity vector for the center-of-mass. Roughly speaking, LAB angles greater than Θ_{CM} represent backward scattering in the CM frame of reference.

The two lower energy angular distributions in figs. 2 and 4 are qualitatively similar. They are both dominated by peaks corresponding to back-scattered v = 4 and v = 3 product. The signal at 0.79 kcal/mole is considerably lower because this collision energy is close to the entrance channel barrier height of the potential energy surface. The peaks are better resolved in this scan than at 1.82 kcal/mole. This is partly due to the smaller v = 4 recoil velocity at the lowest energy, but it also indicates that the product scattering in the center-of-mass is more strongly backward-peaked at 0.79 kcal/mole.

The F + D_2 angular distribution at 3.00 kcal/mole is quite different from the one at 1.82 kcal/mole. The backward-scattered v = 4 and v = 3 peaks are less distinct, there is considerably more forward scattering, and there is a small peak at $\Theta = 10°$ which appears to correspond to v = 4 product scattered near $\theta = 0°$ in the CM. This peak is reminiscent of the forward v = 3 peak observed in the F + H_2 angular scans. At this energy the entire v = 3 circle is within range of the rotating detector. We looked for forward scattered v = 3 product on the other side of the F beam but did not find any.

The F + HD angular distributions are shown in figs. 5-7. It is clear that the HF and DF product angular distributions are not at all alike. The DF angular distributions at all three energies consist mainly of backward-scattered v = 4 and v = 3 product. They resemble the lower energy F + D_2 angular scans. The outstanding feature in the HF angular distributions at 1.98 and 1.35 kcal/mole is a peak corresponding to forward scattered v = 3 product. The back-scattered v = 3 and v = 2 peaks seen in F + H_2 are nearly absent here

although both angular distributions show a small bump that drops off near the backward edge of the v = 3 circle which probably is from a small amount of sideways or backward scattered v = 3. The collision energy at 1.35 kcal/mole is barely above the threshold for v = 3 formation, and the collision energy at 0.8 kcal/mole is well below it. The disappearance of the sharp peak of HF products at 0.8 kcal/mole shows that it is indeed due to HF (v = 3). The signal attributable to HF (v = 2) is rather featureless at all three energies. The v = 2 circle is too large for any forward-peaked product to be within range of the detector. However, no signal was seen on the other side of the F beam at any energy. There is a rise in the signal at 0.82 kcal/mole at LAB angles < 15° which appears at 1.35 kcal/mole as a plateau between the forward v = 3 peak and the F beam. It is apparent to a lesser extent at 1.98 kcal/mole. We are uncertain if this is reactive signal due to sideways scattered v = 2, or if it is an artifact resulting from being too close to the F beam. The two lower energy angular distributions show that the DF signal drops off considerably below 1.35 kcal/mole.

Time-of-flight measurements were taken for F + D_2 at 1.82 and 3.32 kcal/mole, and for F + HD at 1.98 kcal/mole. TOF spectra of the HF product from F + HD could be obtained only at the forward peak because of the low signal-to-noise ratio at most angles, so we were unable to construct a contour map for the HF channel. 16 TOF spectra were taken at each F + D_2 energy, and 12 DF spectra were taken for F + HD. The complete set of TOF spectra is displaced in figs. 8,9, and 10, along with the assignments to product vibrational states obtained by the CM ⇒ LAB analysis.

The TOF spectra for F + D_2 at 1.82 kcal/mole show well-resolved v = 3 and v = 4 peaks at most angles. Two v = 4 peaks are observed at angles that cut across the v = 4 circle, and these peaks merge at angles near Θ = 42° (fig. 8) which is nearly tangent to the circle. At this angle three peaks, corresponding to v = 2, v = 3 and v = 4, are observed, and the v = 2 peak becomes more evident at larger angles. The v = 1 state appears at Θ = 66°(fig. 8) as a fast shoulder at the base of the v = 2 curve. The curves labelled v = 4' will be discussed in the Analysis section.

The resolution of the product vibrational states in the TOF spectra for F + D_2 at 3.32 kcal/mole is considerably worse than at 1.82 kcal/mole since the v = 4 recoil velocity is larger. Nonetheless one can partially resolve vibrational states at all angles. The TOF spectrum at Θ = 10° (fig. 9) shows that most of the forward peak in the angular distribution is due to v = 4. The v = 1 state is evident at more angles than at 1.82 kcal/mole. The DF spectra from F + HD show resolution comparable to the low energy F + D_2 time-of-flight. The resolution is somewhat worse because the v = 4 and v = 3 Newton circles are closer in size.

4. Analysis

The determination of the center-of-mass angular and kinetic energy distributions was done with the same forward convolution procedure as was used for F + H_2. Again, it was necessary to account for the reactant rotational populations in estimating the total available energy for the calculations. This is more of a problem for D_2 than for HD. Rotational relaxation of HD in a supersonic beam is relatively

efficient as the HD can undergo $\Delta J = 1$ transitions which are more facile than the $\Delta J = 2$ transitions required for the homonuclear species, and can result in virtually complete relaxation to $J = 0$. In addition, the displacement between the center-of-mass and the center-of-charge results in a more anisotropic interaction potential for HD which promotes rotational relaxation. From the photo-electron data of Pollard et al. [30] we estimate that greater than 90% of the HD is in $J = 0$ with nearly all the rest in $J = 1$. The exothermicity of 32.9 kcal/mole was used as the total available energy for F + HD → DF + H. The D_2 can, at best, have a $J = 1 : J = 0$ ratio of 1:2, and the restriction to even ΔJ transitions results in less rotational cooling in the expansion. The D_2 populations for the room temperature beam are estimated to be 40% $J = 0$, 30% $J = 1$, 25% $J = 2$, and most of the rest in $J = 3$.

For F + D_2 at 1.82 kcal/mole, the $J = 1$ population was explicitly accounted for by adding 0.2 kcal/mole to the exothermicity in figure 1 resulting in a value of 32.1 kcal/mole for the total available energy. This gave acceptable fits to all the time-of-flight spectra except at $\Theta = 42°$ and $\Theta = 46°$ (fig. 8). These LAB angles are nearly tangent to the DF (v = 4) Newton circle and sample strongly back-scattered v = 4 product. The faster part of the v = 4 peaks at these angles could be fit by assuming a small contribution from the reaction of F with D_2 (J = 2), and this contribution is labelled v = 4'. The analogous TOF spectra for the F+HD reaction, at $\Theta = 40°$ and $\Theta = 42°$ (fig. 10), required no additional state to fit the data. As the HD beam has virtually no rotational excitation, this further supports the claim

that the v = 4' product from F + D_2 and the v = 3' product from F + H_2 shown in the previous paper are from rotationally excited reactants rather than from spin–orbit excited $F(^2P_{1/2})$.

The F + D_2 data at 3.32 kcal/mole could not be fit near the forward or the backward edge of the v = 4 circle with a total available energy of 32.1 kcal/mole, i.e., the exothermicity of F + D_2 (J = 1). The D_2 (J = 2) population in the high temperature beam might be as much as twice the population in the room temperature beam because of the higher stagnation temperature and the lower inverse Knudsen number [30] for the expansion. The J = 2 rotational energy was included in the total available energy as the resolution at this collision energy was too poor to justify as separate v = 4' state.

The computer–generated fits to the F + D_2 LAB angular distributions are shown in figs. 2 and 3. The best fit CM parameters for the three systems are graphically displayed in figs. 11–13. As in the previous paper, the coupled CM recoil energy and angular distribution is given by

$$P_i(E,\theta) \;=\; N_i I_i(\theta) \left(1 - \frac{E}{E_m^i}\right)^{\alpha_i(\theta)} \left(\frac{E}{E_m^i}\right)^{\beta_i(\theta)}$$

with

$$\beta_i(\theta) \;=\; \alpha_i(\theta) \left[\frac{E_p^i(\theta)}{1 - E_p^i(\theta)}\right].$$

$I_i(\theta)$ is the integrated intensity of vibrational state i at θ,

$E_p^i(\theta)$ is the maximum in the recoil energy distributions, and $\alpha_i(\theta)$ determines the width of the recoil energy distribution. E_m^i is the maximum recoil energy for state i, and was chosen for v = 4' assuming $D_2(J=2)$ rotational excitation.

The center-of-mass velocity flux contour maps are displayed in figs. 14-16. The F + HD map shows that all four observed DF vibrational states are backward-peaked. The F + D_2 contour map at 1.82 kcal/mole shows the v = 3, 2, and 1 states peaking at or near 180°. The v = 4 state has a broad sideways peak centered around 130°, and it extends further into the forward hemisphere than the v = 4 state from F + HD. The v = 4' state is scattered entirely into the backward hemisphere.

In the F + D_2 contour map at 3.32 kcal/mole one sees that the v = 3, 2, and 1 distributions have broadened considerably relative to 1.82 kcal/mole. The v = 3 distribution is sideways-peaked at this energy. The v = 4 distribution has changed the most dramatically, however. It has a forward peak at θ = 0°, a sharp dip near 20°, and is almost isotropic for θ > 30°.

The F + D_2 relative partial cross sections for each vibrational state, σ_i, the relative total cross sections $\sigma = \sum_i \sigma_i$, and the normalized partial cross sections $\sigma_i' = \sigma_i/\sigma$ at the two collision energies are shown in figs. 17 and 18. The branching ratios derived from this work for F + D_2 and F + HD as well as some of the results from earlier chemiluminescence work are tabulated in Table 2. The v = 4' and v = 4 contributions have been summed in the cross section graphs and the branching ratio table. The v = 4' partial cross section

is about 10% of that for v = 4 at 1.82 kcal/mole. The reactivity of D_2 (J = 2) relative to lower rotational states cannot be determined definitively because of the difficulty in distinguishing the v = 4 and v = 4' contributions to the TOF spectra. The v = 4' partial cross section represents a lower bound since the data was fit with as little v = 4' as possible.

Table 2 shows that the (v = 4)/(v = 3) and (v = 2)/(v = 3) ratios for F + D_2 at 1.82 kcal/mole and F + HD ⇒ DF + H are somewhat lower than the chemiluminescence values [8]. However, there is not much difference between the F+D_2 and F+HD ratios, and the (v = 4)/(v = 3) ratio is higher than the (v = 2)/(v = 3) ratio for both reactions. These comparisons agree with the chemiluminescence results. The variation of the partial cross sections and branching ratios with collision energy for F + D_2 is similar to that seen for F + H_2 in the previous chapter. All the partial cross sections increase with collision energy, but the (v = 4)/(v = 3) ratio decreases whereas the (v = 2)/(v = 3) ratio increases. For F + H_2 the (v = 3)/(v = 2) ratio decreased and the (v = 1)/(v = 3) ratio increased as the collision energy was raised. Figure 18 shows that the v = 2 and v = 1 products increase at the expense of v = 3 and v = 4 as the energy is raised. The trend in the kinetic energy dependence of the (v = 2)/(v = 3) ratio agrees with the temperature-dependent chemiluminescence results [8] but not with an earlier chemical laser study [6] which showed a significant drop in this ratio with increasing temperature. A decrease in the (v = 4)/(v = 3) ratio does not occur in the chemiluminescence study at the higher temperature.

5. Discussion

The results presented here and in the previous paper show that there are marked differences in the product angular distributions within the set of isotopic reactions (1) to (4). While classical trajectory studies predict a tendency for the angular distributions to become progressively less strongly backward-peaked for the sequence (4) - (1), the extent of the variation observed here seems well beyond what one would expect from a classical calculation on any reasonable potential energy surface. The observed trends in the angular distributions are, on the other hand, readily explained in terms of combinations of direct reactive scattering, which can be reproduced in classical trajectory calculations, and dynamical resonance phenomena.

Reaction (4), $F + HD \rightarrow DF + H$, behaves the most classically of the four reactions. The contour map at 1.98 kcal/mole shows all the product vibrational states to be backward-peaked. This is the expected result for a potential energy surface favoring collinear approach of the reactants. The rapid fall-off in the product yield as the collision energy is lowered from 1.35 to 0.82 kcal/mole is consistent with the behavior expected for a direct reaction at collision energies near the mechanical barrier for reaction, although it is possible that the contribution from tunneling is important at the lowest energy.

One difference between reaction (4) and the $F + H_2$ and D_2 reactions is that the quantal collinear calcuations on M5 do not predict nearly as much of a delayed onset for DF ($v = 4$) product from (4) as they do for DF ($v = 4$) from $F + D_2$ and HF ($v = 3$) from $F + H_2$ [19]. The delayed onset refers to the energy difference between where a product

vibrational state is energetically accessible and where it first appears in the scattering calculation, and it is thought to be due to a $v = 4$ or, for $F + H_2$, a $v = 3$ adiabatic barrier in the product valley of the potential energy surface [22]. The 1 kcal/mole additional exothermicity of reaction (4) relative to (3) reduces the effect of the $v = 4$ barrier for (4). The observation of $v = 4$ product from (4) at 0.82 kcal/mole therefore does not contradict the results of the M5 calculations. However, the $F + D_2$ distribution at 0.78 kcal/mole also shows $v = 4$ product even though the M5 collinear calculations predict a delayed onset of > 1 kcal/mole. This again indicates that the M5 surface should be modified so as the reduce to $v = 4$ exit barrier. For $F + H_2$, it was suggested in the previous chapter that lowering the $v = 3$ exit barrier would cause resonance effects to appear in the $v = 3$ product rather than $v = 2$ as predicted on M5. Similarly, the DF ($v = 4$) product might be expected to be influenced by resonances rather than $v = 3$ once the $v = 4$ barrier is lowered.

Our results for $F + D_2$ indeed suggest that this is occurring. The contour map at 1.82 kcal/mole shows that the $v = 4$ product, while predominantly scattered into the backward hemisphere, shows sideways peaking. At the higher energy, the angular distributions for all four observed vibrational states are broader, which is the expected classical result as more non-collinear collisions contribute to the reaction. However, the $v = 4$ distribution is considerably different from the others since it is the only one showing a forward peak. This resembles the behavior calculated for $F + H_2$ on M5 in which backward-scattering occurred at 2 kcal/mole collision energy, and, when

the collision energy was raised to 3 kcal/mole, the resonance-enhanced contribution to reaction at higher impact parameters resulted in a state-selective broadening of HF (v = 2). The experimental results, on the other hand, showed forward-peaked v = 3 from F + H_2 at collision energies as low as 0.7 kcal/mole. This was attributed to the $\underline{L}$ = 0 resonance being below the lowest collision energy. If the v = 4 scattering for F + D_2 is interpreted in terms of dynamical resonances, the results suggest that the $\underline{L}$ = 0 resonance energy is higher than for F + H_2. Thus, if the resonance is being accessed at all at 1.82 kcal/mole, it is probably being formed only by low impact parameter collisions which result in a primarily back-scattered angular distribution. The forward scattering occurs at the higher energy where the resonance can be accessed only by higher $\underline{L}$ collisions.

The quantal collinear calculations predict the lowest resonance for F + D_2 to be higher relative to the reactant zero point energy than for F + H_2 since the adiabatic curve supporting the quasi-bound state is considerably shallower [21,29], and our experimental results for F + H_2 and F + D_2 agree with this. The calculations also predict a shorter lifetime for the F + D_2 resonance, and the larger skew angle for F + D_2 should result in more direct vs. resonant scattering than for F + H_2. The contour map for F + D_2 at 3 kcal/mole shows far less forward scattering than any of the F + H_2 contour maps, and this is consistent with the implications of the collinear results.

Although the results for reactions (2) – (4) can be explained in terms of dynamical resonances and the 'resonance hierarchy' inferred from the collinear calculations, the F + D_2 and F + HD $\rightarrow$ DF + H

results considered by themselves might not be considered sufficient proof for the existence of resonance effects. The stronger backward-scattering for DF (v = 4) from F + HD compared to F + D_2 at 1.82 kcal/mole might be due to the greater contribution of small impact parameter collisions to F + HD because the center-of mass of HD is closer to the D atom. The forward-scattering of v = 4 at 3.32 kcal/mole is accompanied by sideways-peaked v = 3 product, so the broadening of the angular distribution is not nearly as state-specific as for F + H_2. Indeed, it is conceivable that a classical trajectory calculation using a reasonable potential energy surface could reproduce many important features of the high energy F + D_2 angular distribution.

Classical trajectory calculations on the M5 surface result in much stronger backward peaking of DF product at higher collision energies than our results indicate. This difference arises largely from too high a bending force constant on M5. The correct potential energy surface should have a lower bending force constant, as the ab initio PES calculation also indicates.

The results for F + HD $\rightarrow$ HF + D, on the other hand, almost force one to think in terms of dynamical resonances. The most prominent feature in these angular distributions is a forward-scattered v = 3 peak even at a collision energy just above the v = 3 threshold. This bears very little resemblance to angular distributions derived from classical trajectory studies. The collinear quantal calculation on M5 predicts a strong, low energy resonance leading to v = 2 and very little direct scattering. Extensing to three dimensions, (one would expect extensive forward or sideways scattering in the angular distribution reflecting

the dominant contribution from high impact parameter collisions at energies above the $\underline{L} = 0$ resonance. This is just what we see in our angular distributions, although, as with $F + H_2$, HF ($v = 3$) is the observed product of the resonance rather than $v = 2$.

The collinear resonance for $F + HD \rightarrow HF + D$ on M5 is only about 0.2 kcal/mole above the reactant zero-point energy and is about 1 kcal/mole below the HF($v = 3$) threshold [19]. The bending zero point energy for FHD on M5 is around 1 kcal/mole [9,11], so the $\underline{L} = 0$ resonance energy in three dimensions should be quite close to the $v = 3$ threshold which in turn, is close to the collision energy of 1.35 kcal/mole in one of the experiments. The forward peak observed at this energy indicates that the true $\underline{L} = 0$ resonance energy should be lower than is predicted on the M5 surface, as was the case with $F + H_2$. The $\underline{L} = 0$ resonance energy could be lowered by reducing the bending zero-point energy or by increasing the depth of the adiabatic well. This last step is likely to lower the collinear resonance below the reactant zero-point energy, in which case it will not show up in a collinear calculation.

The extent of the correspondence between the collinear calculation and the angular distributions for (1) is somewhat exaggerated by the reaction kinematics. The nearly total absence of direct reaction in the collinear calculation is largely due to the small skew angle, and the suppression of direct scattering should be less for non-collinear collisions. Indeed, the IR chemiluminescence studies [8] showed that $v = 2$ was the dominant product for this reaction. We cannot calculate branching ratios due to the lack of TOF data, but our angular scans

are not as inconsistent with this result as it might seem at first glance. The intensity transformation from CM flux to LAB number density is proportional to v/u^2,[30] where v is the LAB velocity and u is the CM velocity for the detected product. The v = 2 circle is much larger than the v = 3 circle for this reaction at 1.98 and 1.35 kcal/mole, and the u^{-2} term reduces the (v = 2)/(v = 3) LAB intensity by a factor of 16 at 1.98 kcal/mole and 70 at 1.35 kcal/mole. Thus the CM v = 2 flux is far higher than it appears in the angular distributions. The form of the v = 2 CM angular distribution is open to speculation. The LAB angular distributions suggest it is quite spread out rather than strongly backward-peaked. It was mentioned previously that forward-peaked v = 2 product would be outside the angular range of our detector. The possibility that the v = 2 product is strongly influenced by resonances cannot be excluded. In any case, while it may not be true that resonance scattering dominates the entire angular distribution as implied by the collinear calculation, it does appear that the v = 3 scattering is dominated by resonance effects to a much greater extent than in $F + H_2$.

Aside from the reduction of the adiabatic exit barrier for the HF (v = 3) and DF (v = 4) channels in the $F + H_2$ and $F + D_2$ reactions and the decrease of the bending force constant, our studies of the translational energy dependence of this series of reactions do suggest a lower value for the entrance channel potential energy barrier. For example, in the $F + D_2$ reaction the cross section drops rapidly when the collision energy is reduced below 1 kcal/mole. The lowest collision energy for whcih we can obtain an angular

distribution is 0.79 kcal/mole. (At 0.69 kcal/mole the signal level is too low.) We expect that the correct PES should give a threshold of 0.75 ± 0.05 kcal//mole for the $F + D_2$ reaction. More recent rate constant measurements also suggest that the activation energy used in the derivation of M5 is too high [11]. Improved surfaces which incorporate many of our new experimental findings and some ab initio results are starting to appear [33].

6. Conclusion

The variation in the angular distributions for the isotopic set of $F + H_2$ reactions is far greater than predicted by classical calculations. It is, however, quite consistent with the resonance hierarchy predicted in quantal reactive scattering calculations. This underlines the importance of dynamical resonances in these reactions, and supports the claim that resonances in reactive scattering. The effects from resonances appear to be very strong for $F + HD \rightarrow HF$ (v = 3) + D, progressively weaker for $F + H_2 \rightarrow HF$ (v = 3) + H and $F + D_2 \rightarrow DF$ (v = 4) + D, and do not show up at all in $F + HD \rightarrow DF + H$ at the energies studied here.

The changes in the critical region of the M5 surface suggested in the $F + H_2$ studies appear even more reasonable in light of the results presented here.

Acknowledgment

References

[1] A. Persky, J. Chem. Phys. 59 (7) (1973) 3612; 59 (10) (1973) 5578.

[2] M.J. Berry, J. Chem. Phys. 59 (12) (1973) 6229.

[3] E.R. Grant and J.W. Root, J. Chem. Phys. 63 (7) (1975) 2970.

[4] E. Wurzberg and P. L. Houston, J. Chem. Phys. 72 (9) (1980) 4811.

[5] R.F. Heidner, III, J.F. Bott., C.E. Gardner, and J.E. Melzer, J. Chem. Phys. 72 (9) (1980) 4815.

[6] R.D. Coombe and G.C. Pimentel, J. Chem. Phys. 59 (1) (1973) 251.

[7] J. C. Polanyi and K. B. Woodall, J. Chem. Phys. 57 (4) (1972) 1574.

[8] D.S. Perry and J.C. Polanyi, Chem. Phys. 12 (1976) 419.

[9] J.T. Muckerman, J. Chem. Phys. 54 (3) (1971) 1155; 56 (6) (1972) 2997.

[10] J.C. Polanyi and J.L. Schreiber, Chem. Phys. 31 (1978) 113.

[11] J.T. Muckerman, in Theoretical Chemistry – Advances and Perspectives, edited by H. Eyring and d. Henderson (Academic Press, New York, 1981), Vol. 6A, 1–77.

[12] K.P. Huber and G. Herzberg, Constants of Diatomic Molecules (Van Nostrand Reinhold Company, 1979).

[13] D.S. Perry and J.C. Polanyi, Chem. Phys. 12 (1976) 37.

[14] R.K. Sparks, C.C. Hayden, K. Shobatake, D.M. Neumark, and Y.T. Lee, in Horizons in Quantum Chemistry, edited by K. Fukui and D. Pullman (D. Reidel Publishing Co., 1980) 91–105.

[15] T.P. Schafer, P.E. Siska, J.M. Parson, Y.C. Wong, and Y.T. Lee,
      J. Chem. Phys. 53 (1970) 3385.

[16] T.P. Schafer, Ph.D. Thesis, University of Chicago, (1972).

[17] J.C. Polanyi and J.L. Schreiber, Discuss. Faraday Soc. 62 (1977)
      267.

[18] S. Ron, M. Baer, and E. Pollak, J. Chem. Phys. 78 (7) (1983)
      4414; 79 (10) (1983) 5204.

[19] G.C. Schatz, J.M. Bowman, and A. Kuppermann, J. Chem. Phys. 63
      (2) (1975) 685; 63 (2) (1975) 674.

[20] Figure 1, previous paper.

[21] M.S. Child, Molecular Collision Theory (Academic Press, London,
      1974) 211-217.

[22] R.A. Marcus, J. Chem. Phys. 45 (12) (1966) 4500.

[23] V.K. Babamov and A. Kuppermann, J. Chem. Phys. 77 (4) (1982)
      1891.

[24] E. Pollak, J. Chem. Phys. 74 (10) (1981) 5586.

[25] M.J. Redmon and R.E. Wyatt, Chem. Phys. Lett. 63 (2) (1979) 209.

[26] R.E. Wyatt, J.F. McNutt, and M.J. Redmon, Ber. Bunsenges. Phys.
      Chem. 86 (1982) 437.

[27] M. Baer, J. Jellinek, and D. J. Kouri, J. Chem. Phys. 78 (6)
      (1983) 2962.

[28] E.F. Hayes and R.B. Walker, to be published.

[29] K.T. Lee and J.M. Bowman, J. Phys. Chem. 86 (1982) 2289.

[30] J.E. Pollard, D.J. Trevor, Y.T. Lee, and D.A. Shirley, J. Chem.
      Phys. 77 (10) (1982) 4818.

[31] A. Kuppermann and J.A. Kaye, J. Phys. Chem. 85 (1981) 1969.

[32] T.T. Warnock and R.B. Bernstein, J. Chem. Phys. 49 (4) (1968) 1878.

[33] D. G. Truhlar, B. C. Garrett and N. C. Blais, J. Chem. Phys. 80 (1984) 232. Private communications with D. G. Trular and J. T. Muckerman.

Table 1
D$_2$, HD source conditions for the angular scans

Reaction	Source temp($^\circ$K)	Source pressure (psig)	beam velocity ($\times 10^4$ cm/s)	collision energy (kcal/mole)
F+D$_2$	104	45	11.1	0.79
F+D$_2$	307	80	19.6	1.82
F+D$_2$	579	110	27.6	3.32
F+HD	111	45	13.9	0.82
F+HD	185	55	18.4	1.35
F+HD	307	80	23.7	1.98

Table 2
DF product branching ratios for F+D$_2$ and F+HD

	F+D$_2$ 1.82	F+D$_2$ 3.32	F+HD 1.98	F+D$_2$ (ref.8)	F+HD (ref.8)
v=1/v=3	0.02	0.19	0.02	0.15	0.18
v=2/v=3	0.44	0.67	0.40	0.52	0.54
v=4/v=3	0.49	0.41	0.48	0.59	0.61

Figure captions

Fig. 1   Energetics of the $F + H_2$, $F + D_2$, and $F + HD$ reactions. All values are in kcal/mole. H_2, D_2, and HD are in their lowest internal states $(v = 0, J = 0)$.

Fig. 2   LAB angular distribution for $F + D_2$, 1.82 kcal/mole, showing computer-generated fit (● data, ————— total calculated, —— - - - —— $v = 1$, ——— ——— ——— $v = 2$, ———————— $v = 3$, ——— - —— $v=4$, —— ——— —— $v = 4'$).

Fig. 3   LAB angular distribution for $F + D_2$, 3.32 kcal/mole, showing computer-generated fit (no $v = 4'$ state here).

Fig. 4   LAB angular distribution for $F + D_2$, 0.79 kcal/mole.

Fig. 5   LAB angular distribution for $F + HD$, 1.98 kcal/mole (—— —— HF product, Δ - - - - - DF product). The Newton circles corresponding to HF and DF product are drawn with the same texture as the lines in the angular distributions. The HF($v = 3$) and $v = 2$ circles are shown, as are the $v = 4$, 3, and 2 circles for DF.

Fig. 6   LAB angular distributions for F+HD, 1.35 kcal/mole.

Fig. 7   LAB angular distributions for F + HD, 0.82 kcal/mole.   No
HF(v = 3) circle appears as this state is energetically inaccessible.

Fig. 8   Time-of-flight spectra for F + D_2, 1.82 kcal/mole(Δ data,
————— total calculated, —— ——— —— v = 1, —— —— —— v = 2,
——————— v = 3, —— – —— v = 4, —— —— —— v = 4'). Solid
line not shown when it obscures a vibrational state.

Fig. 9   Time-of-flight spectra for F + D_2, 3.32 kcal/mole.

Fig. 10   Time-of-flight spectra for F + HD, 1.98 kcal/mole.

Fig. 11   Best-fit CM parameters for F + D_2, 1.82 kcal/mole
(————— total (top graph only), —— ——— —— v = 1, —— —— ——
v = 2, ——————— v = 3, —— – —— v = 4, —— —— —— v = 4').

Fig. 12   Best-fit CM parameters for F + D_2, 3.32 kcal/mole.

Fig. 13   Best-fit CM parameters for F + HD, 1.98 kcal/mole.

Fig. 14   Center-of-mass velocity flux contour map for F + D_2,
1.82 kcal/mole.

Fig. 15   Center-of-mass velocity flux contour map for F + D$_2$,
3.32 kcal/mole.

Fig. 16   Center-of-mass velocity flux contour map for F + HD,
1.98 kcal/mole.

Fig. 17   Relative total and partial cross sections for F + D$_2$
(——— total, —— --- —— v = 1, —— —— —— v = 2,
-------- v = 3, —— - —— v = 4 (4' added at 1.82 kcal/mole)).

Fig. 18   Normalized cross sections for F + D$_2$.
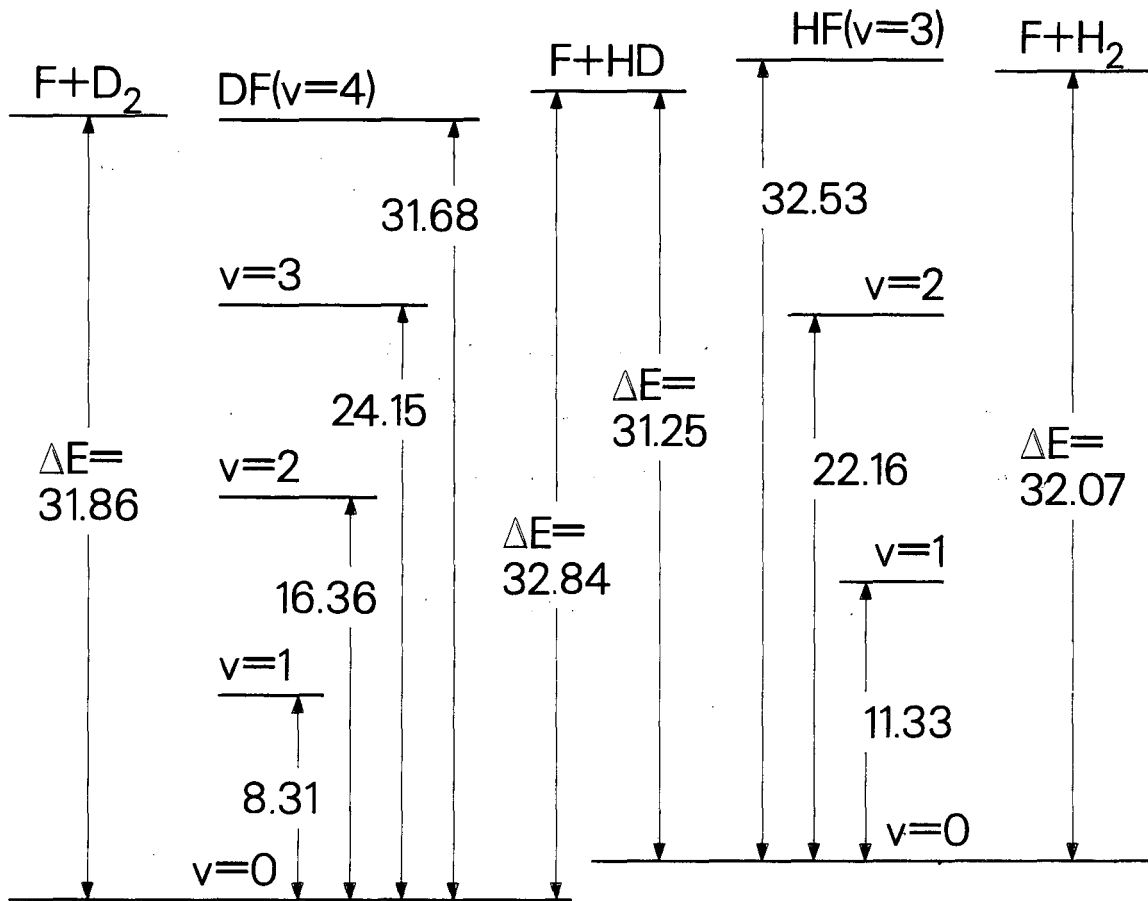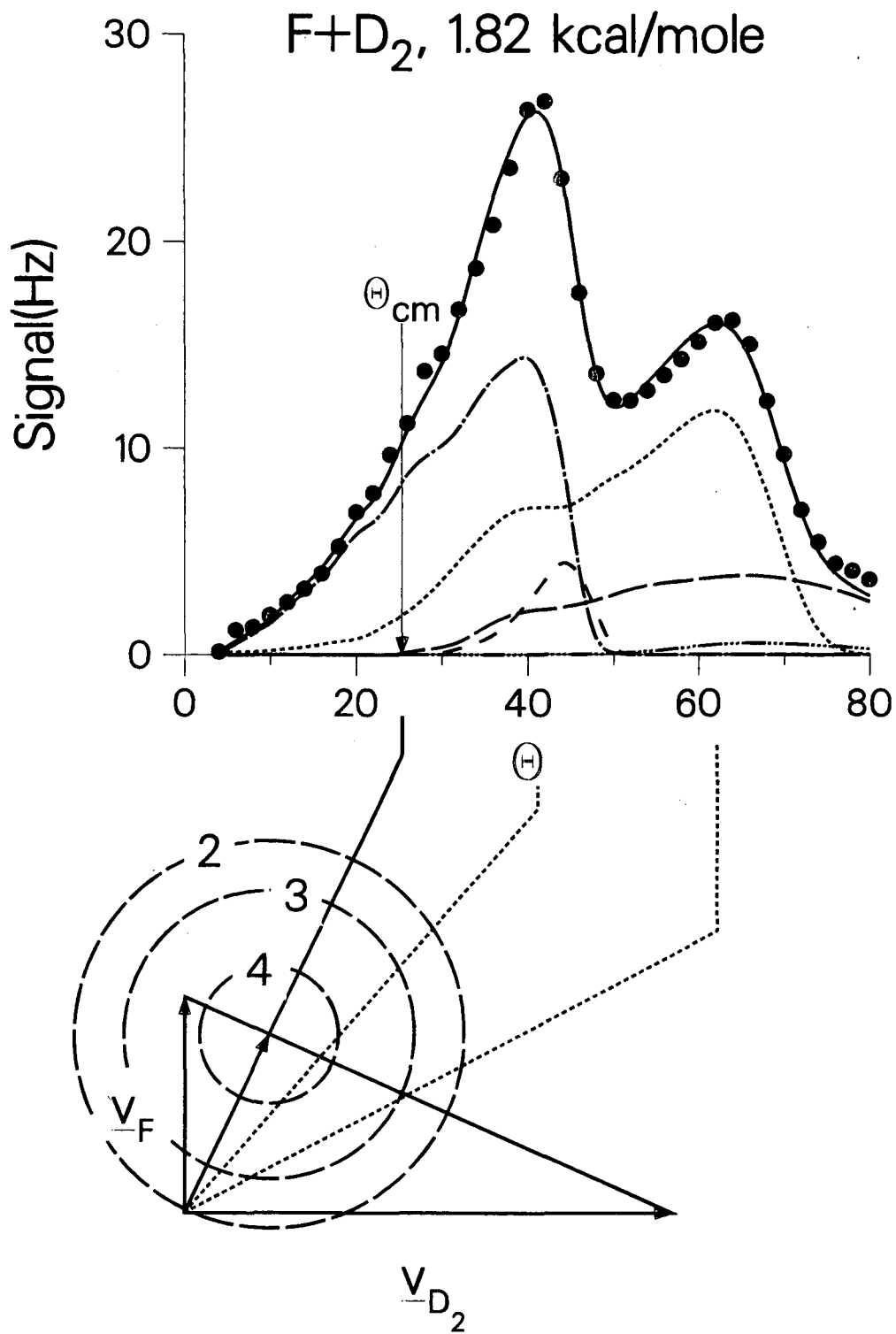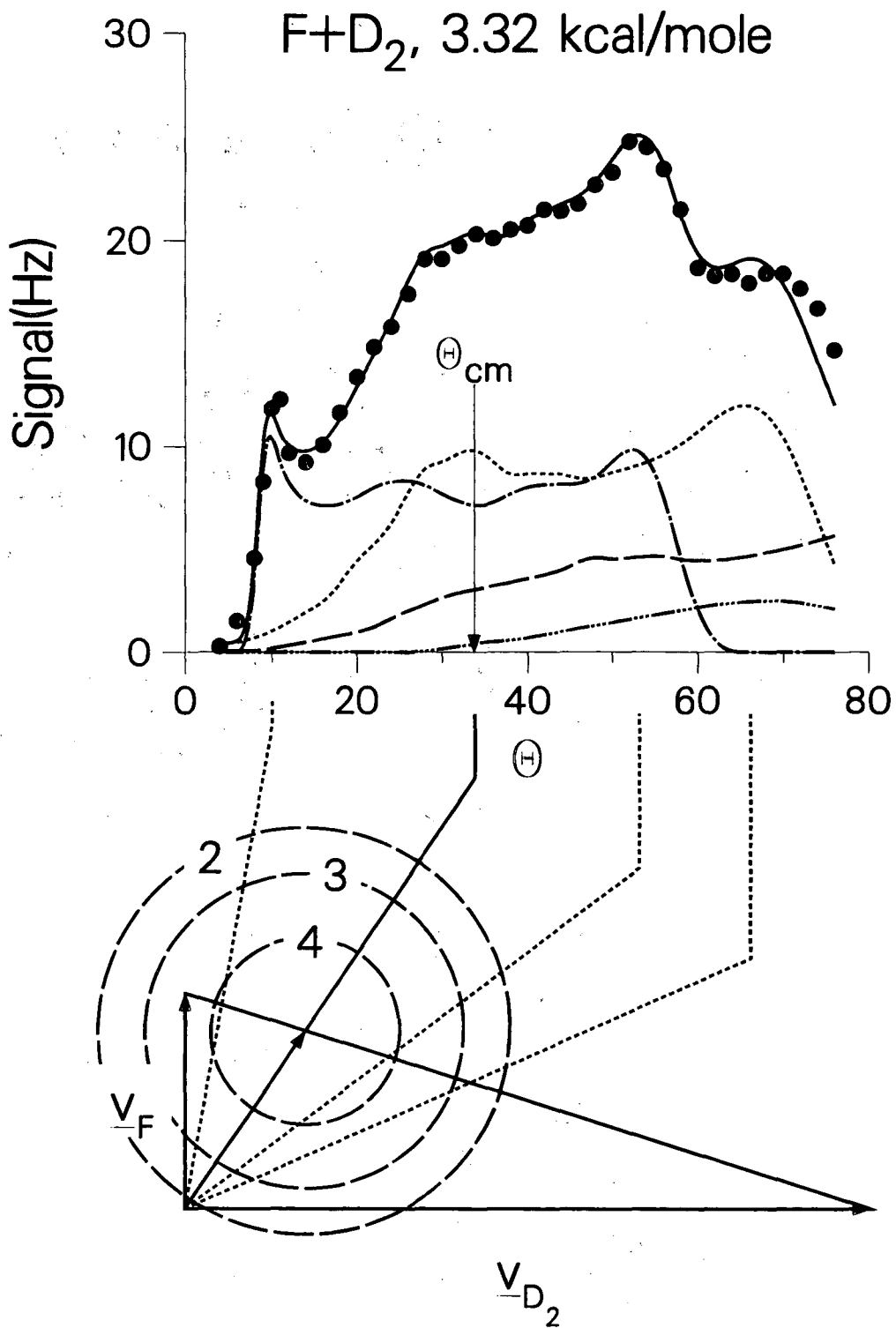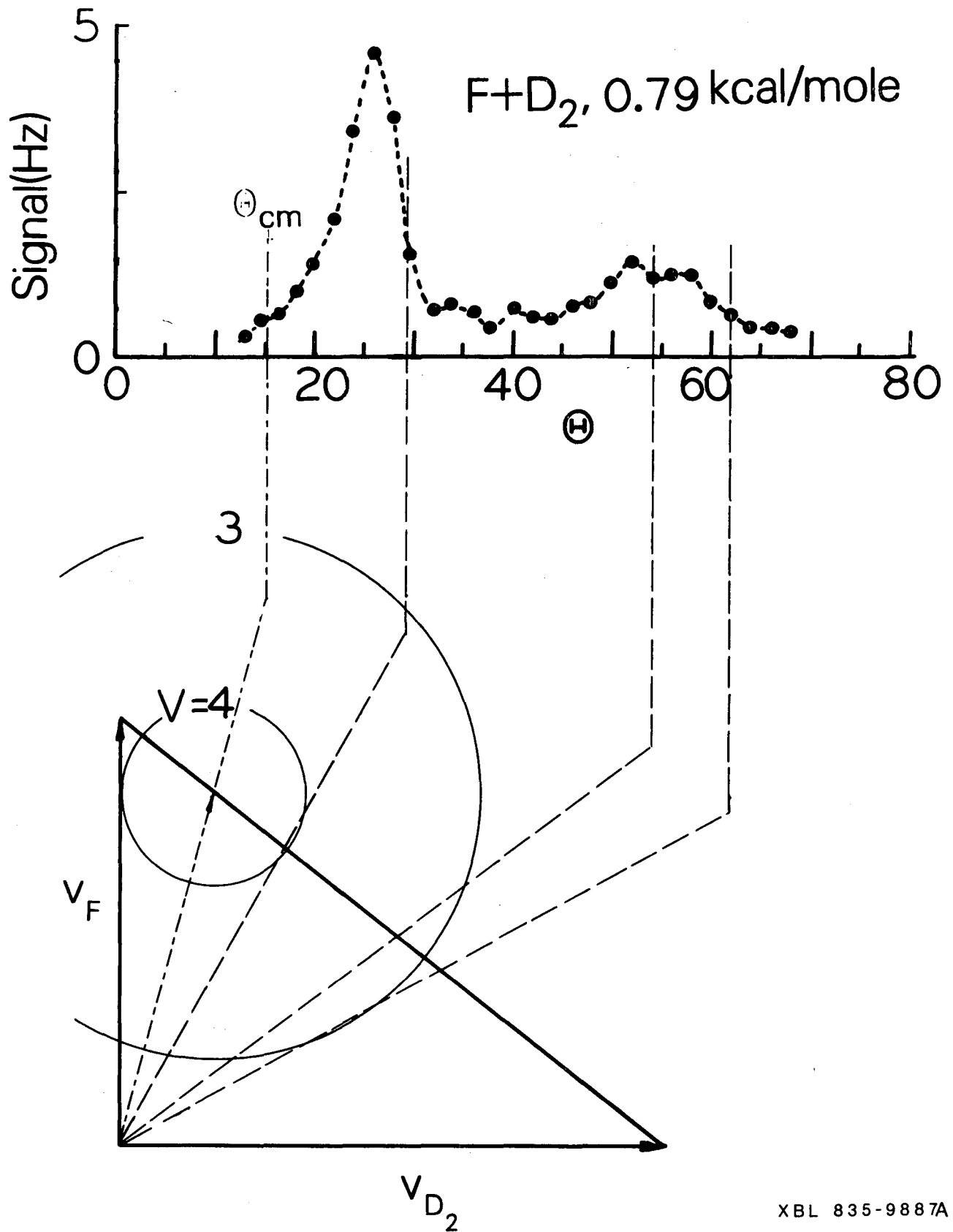
F+D$_2$ DF(v=4)   F+HD   HF(v=3)   F+H$_2$

31.68

v=3

ΔE=
31.86

24.15

ΔE=
31.25

v=2   v=2

16.36   22.16

ΔE=
32.84   v=1

v=1

ΔE=
32.07

8.31   11.33

v=0   v=0

XBL 841-101

Fig. 1

F+D$_2$, 1.82 kcal/mole

Fig. 2

XBL 841-100

F+D$_2$, 3.32 kcal/mole

Fig. 3

XBL 841-98

Fig. 4

XBL 835-9887A

Fig. 5

XBL 841-72

F+HD

1.35 kcal/mole

Fig. 6

XBL 841-97

Fig. 7

XBL 841-99

F+D$_2$→DF+D, 1.82 kcal/mole

N(t) (arb. units)

t/μsec   t/μsec

Fig. 8a

F+D$_2$→DF+D, 1.82 kcal/mole

N(t) (arb. units)

t/μsec   t/μsec

Fig. 8b

F+D$_2$→DF+D, 1.82 kcal/mole

Fig. 8c

XBL 841-81

38

F+D$_2$→DF+D, 3.32 kcal/mole

10°   20°

12°   24°

16°   28°

N(t) (arb. units)

t/μsec   t/μsec

XBL 841-82

Fig. 9a

$F+D_2 \rightarrow DF+D$, 3.32 kcal/mole

XBL 841-84

Fig. 9b

F+D$_2$→DF+D, 3.32 kcal/mole

Fig. 9c

41

F+HD→DF+H, 1.98 kcal/mole

XBL 841-85

Fig. 10a

42

F+HD→DF+H, 1.98 kcal/mole

XBL 841-71

Fig. 10b

F+D$_2$→DF+D, 1.82 kcal/mole

Fig. 11

F+D$_2$→DF+D, 3.32 kcal/mole

XBL 841-87

Fig. 12

F+HD→DF+H, 1.98 kcal/mole

Fig. 13

F+D$_2$→DF+D, 1.82 kcal/mole

Fig. 14

F+D$_2$→DF+D, 3.32 kcal/mole

0°

v=1
v=2
v=3
v=4

XBL 841-110

Fig. 15

48

F+HD→DF+H, 1.98 kcal/mole

v=1

v=2

v=3

v=4

0°
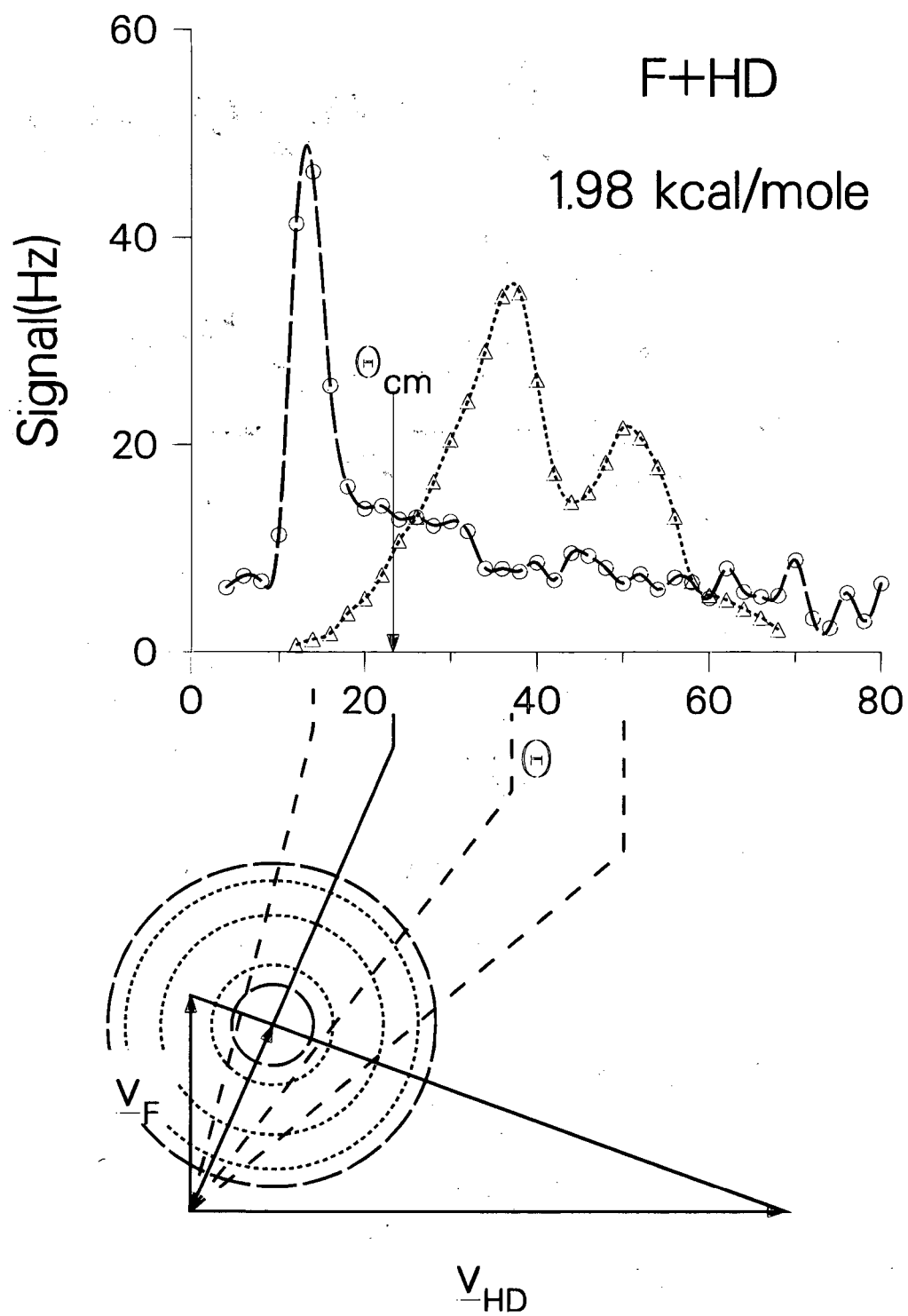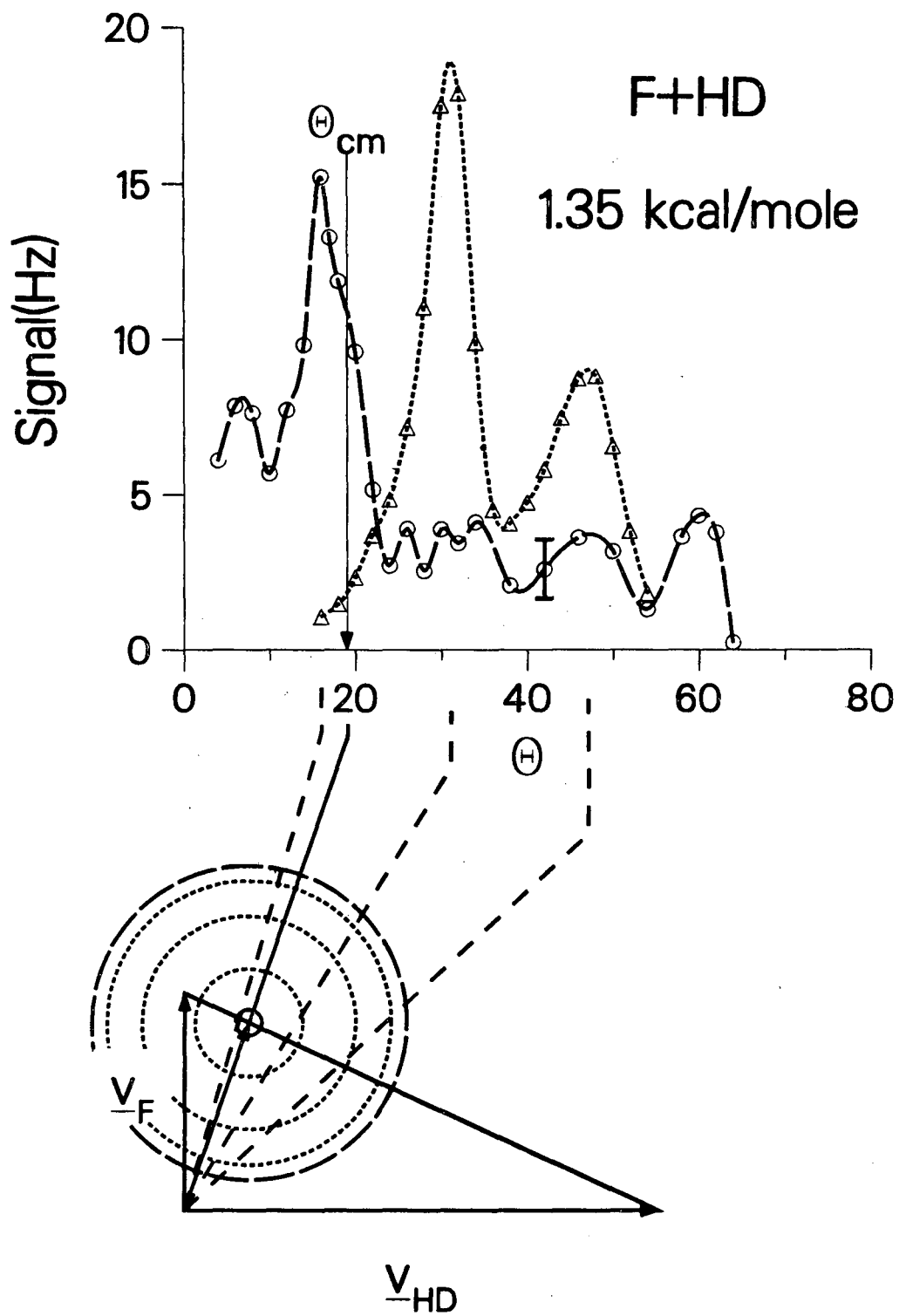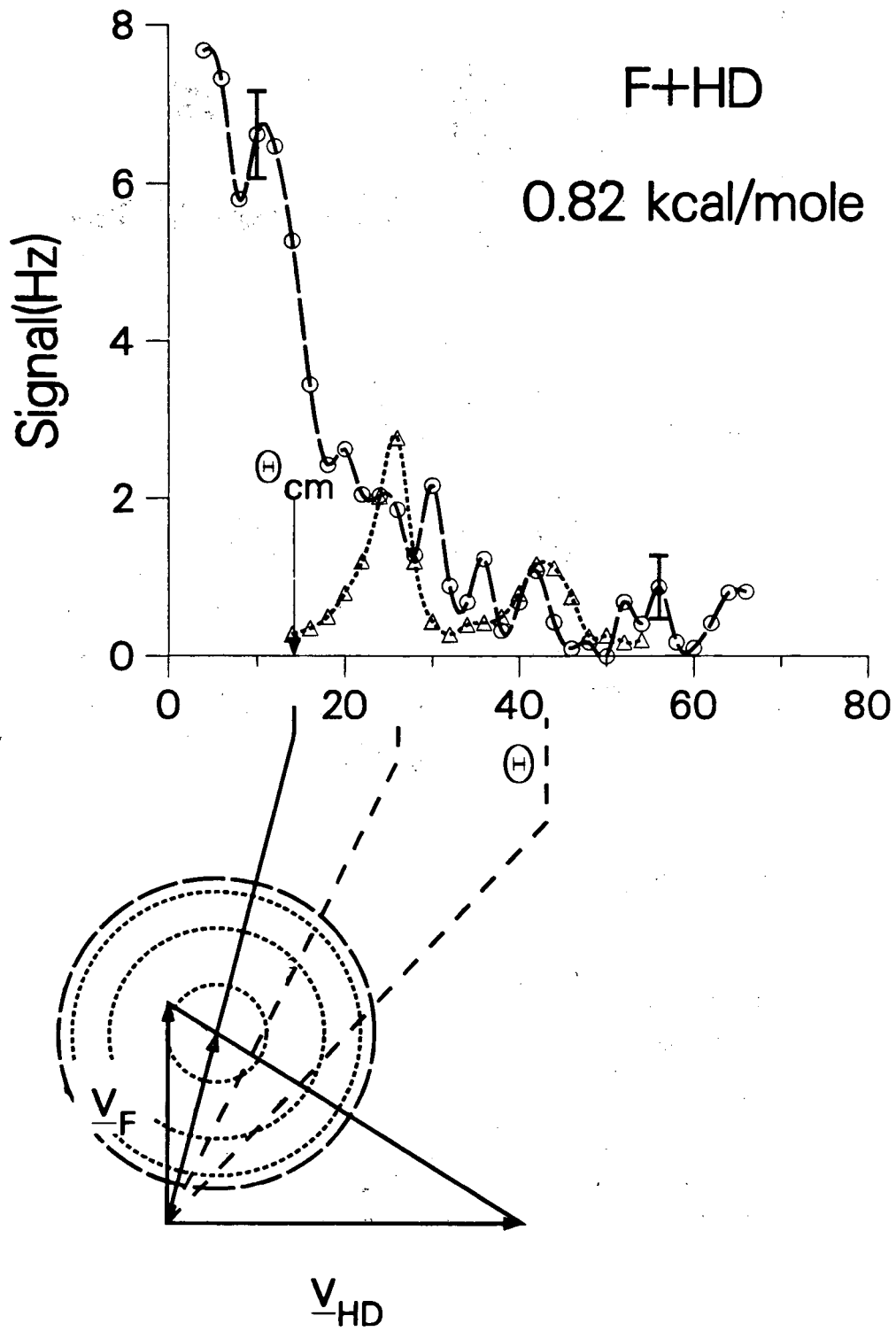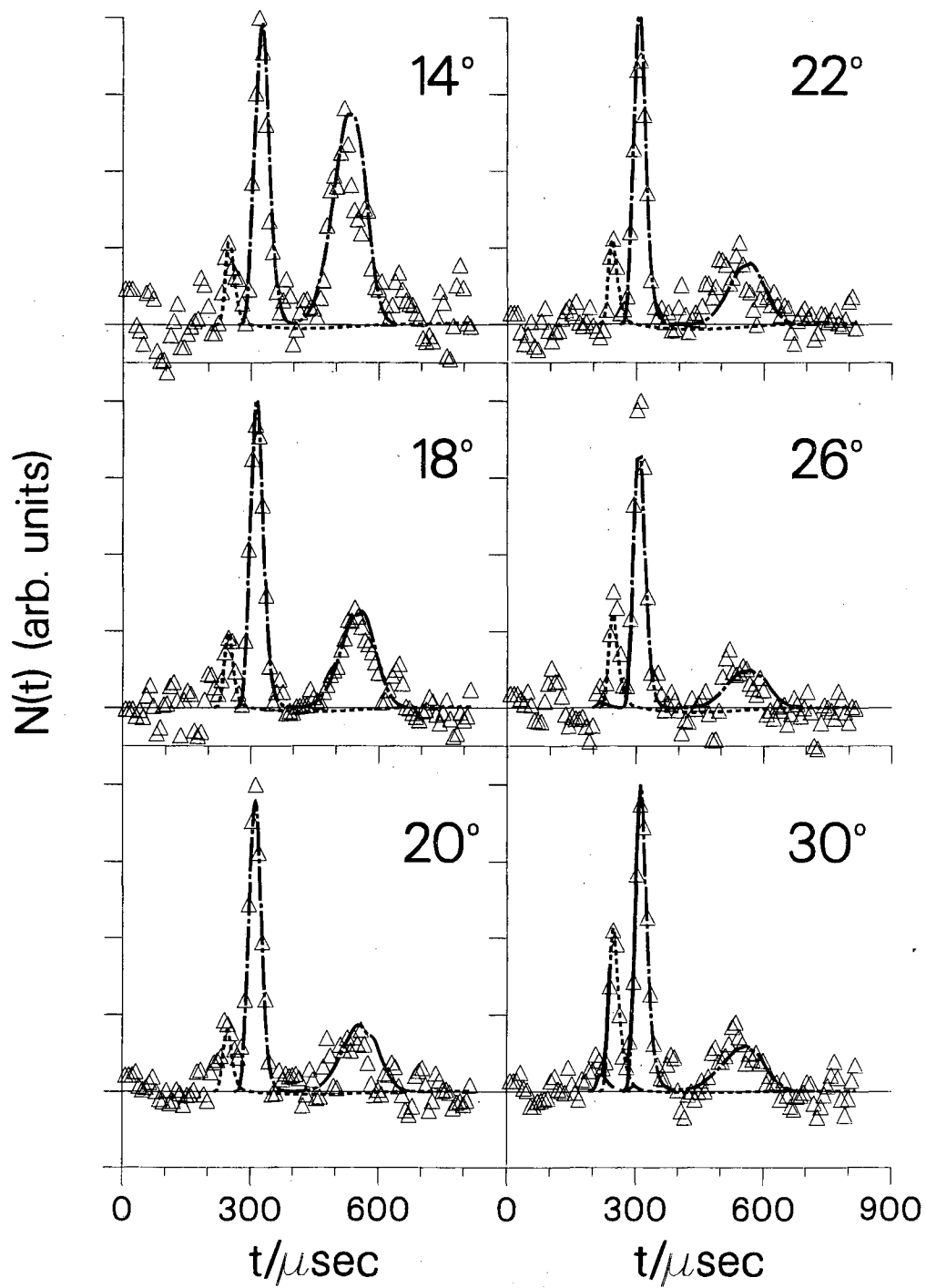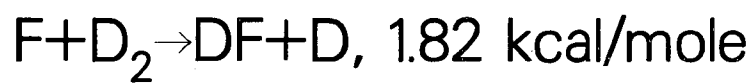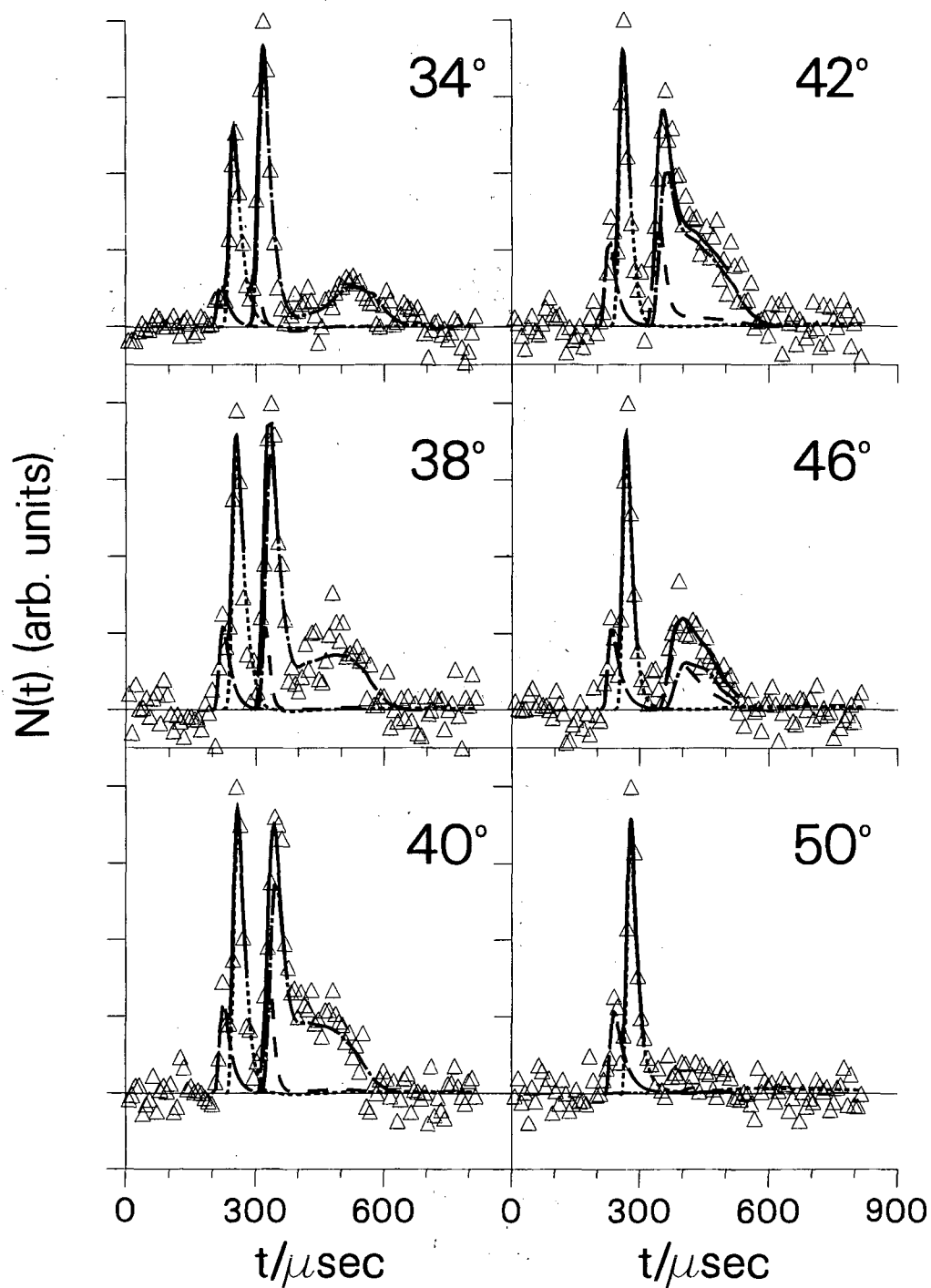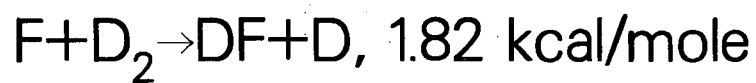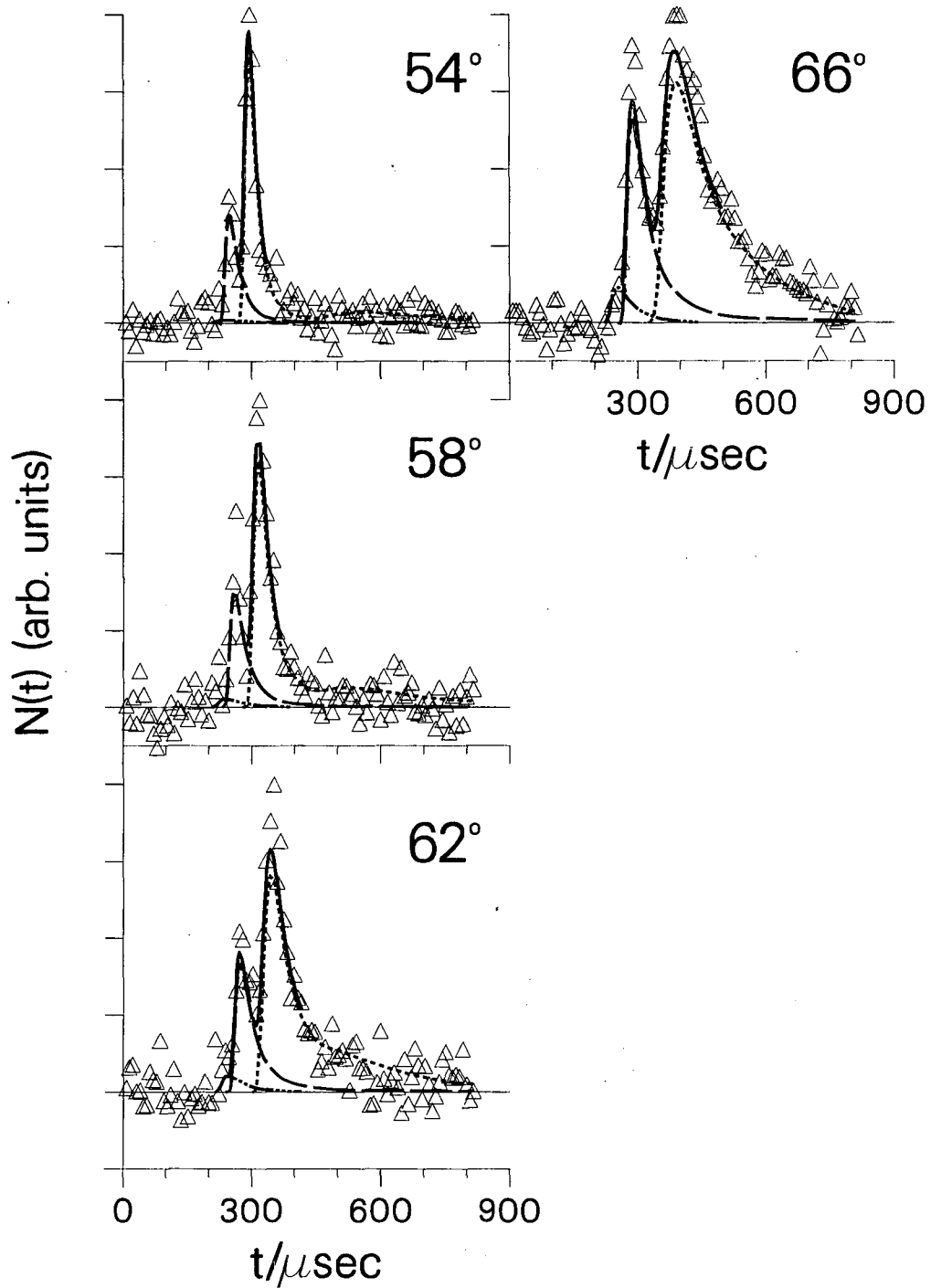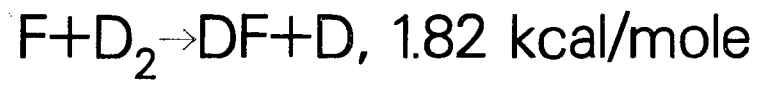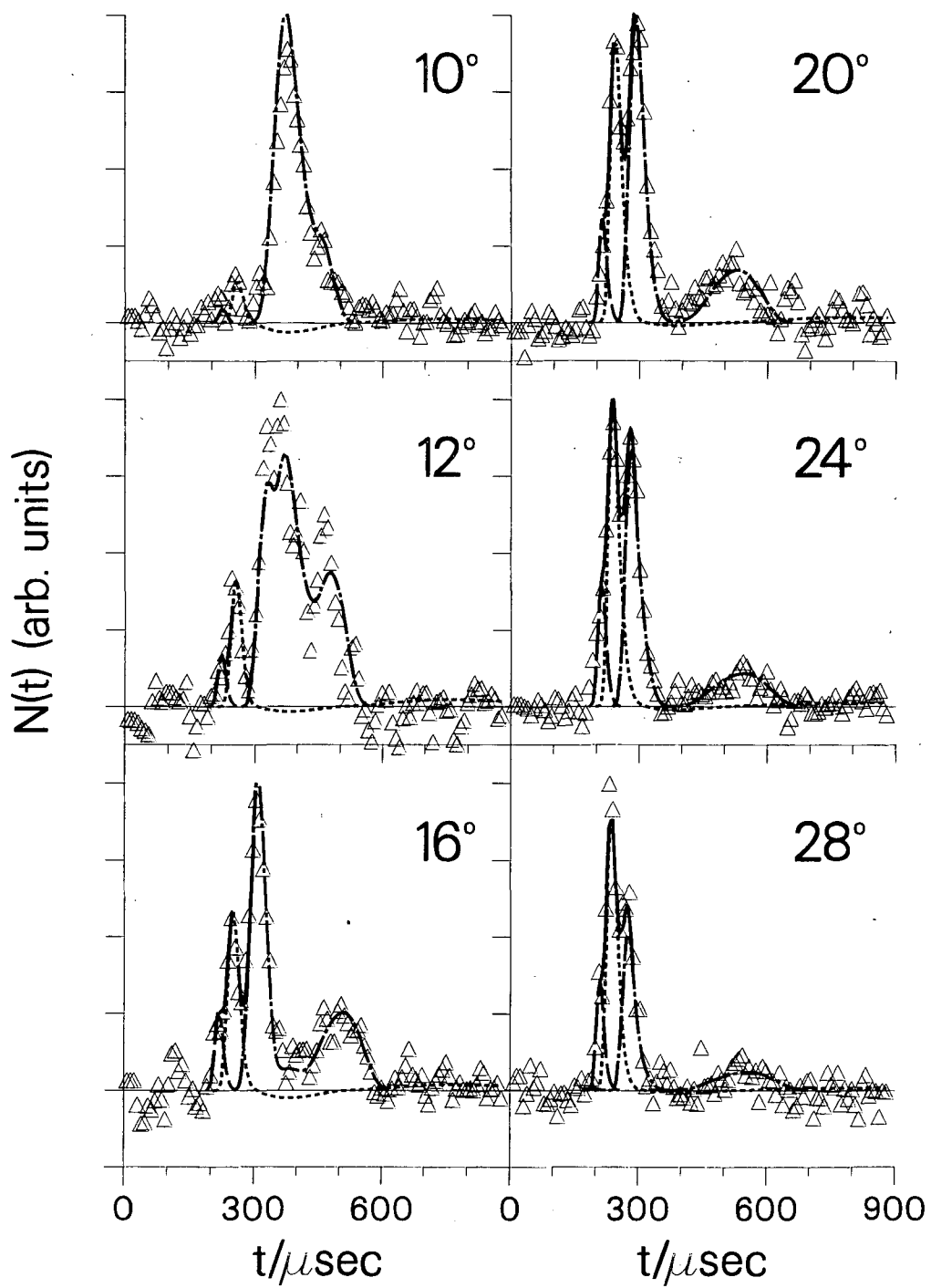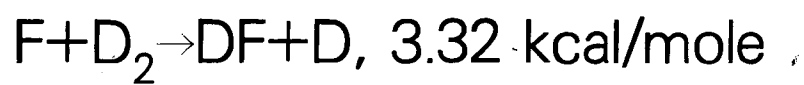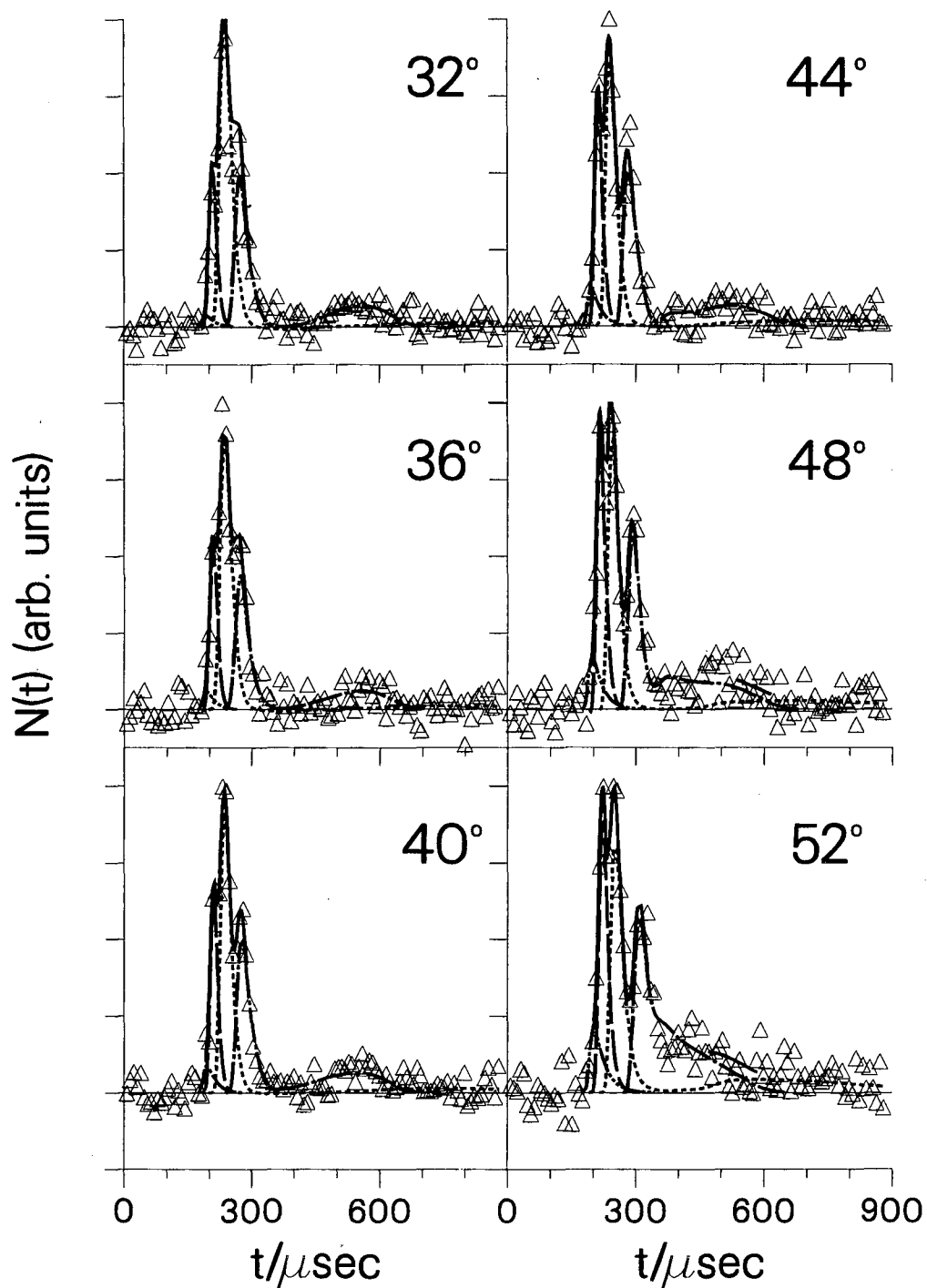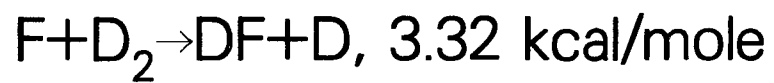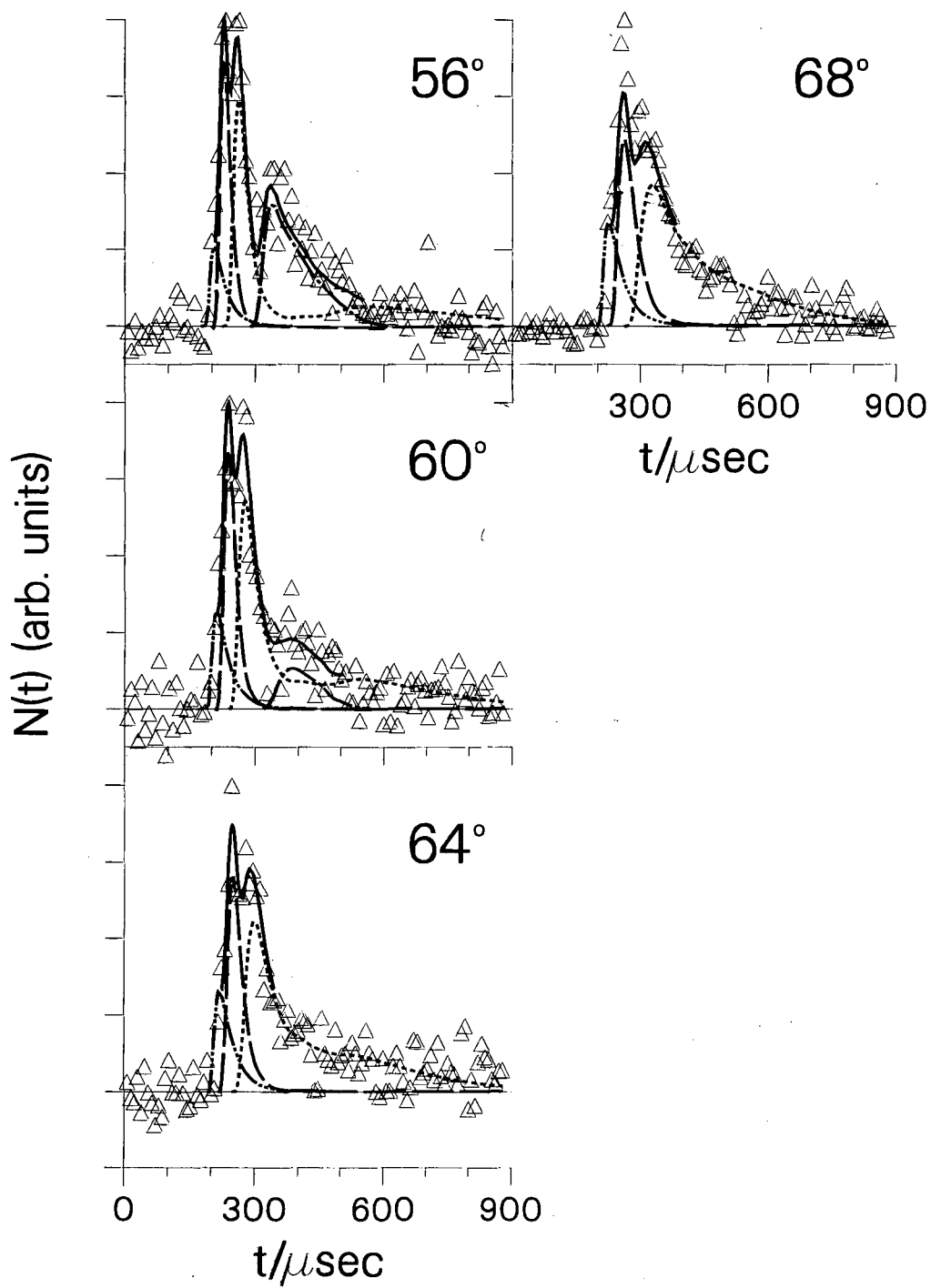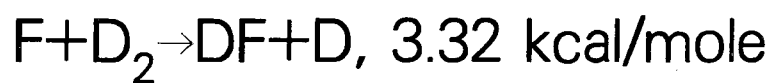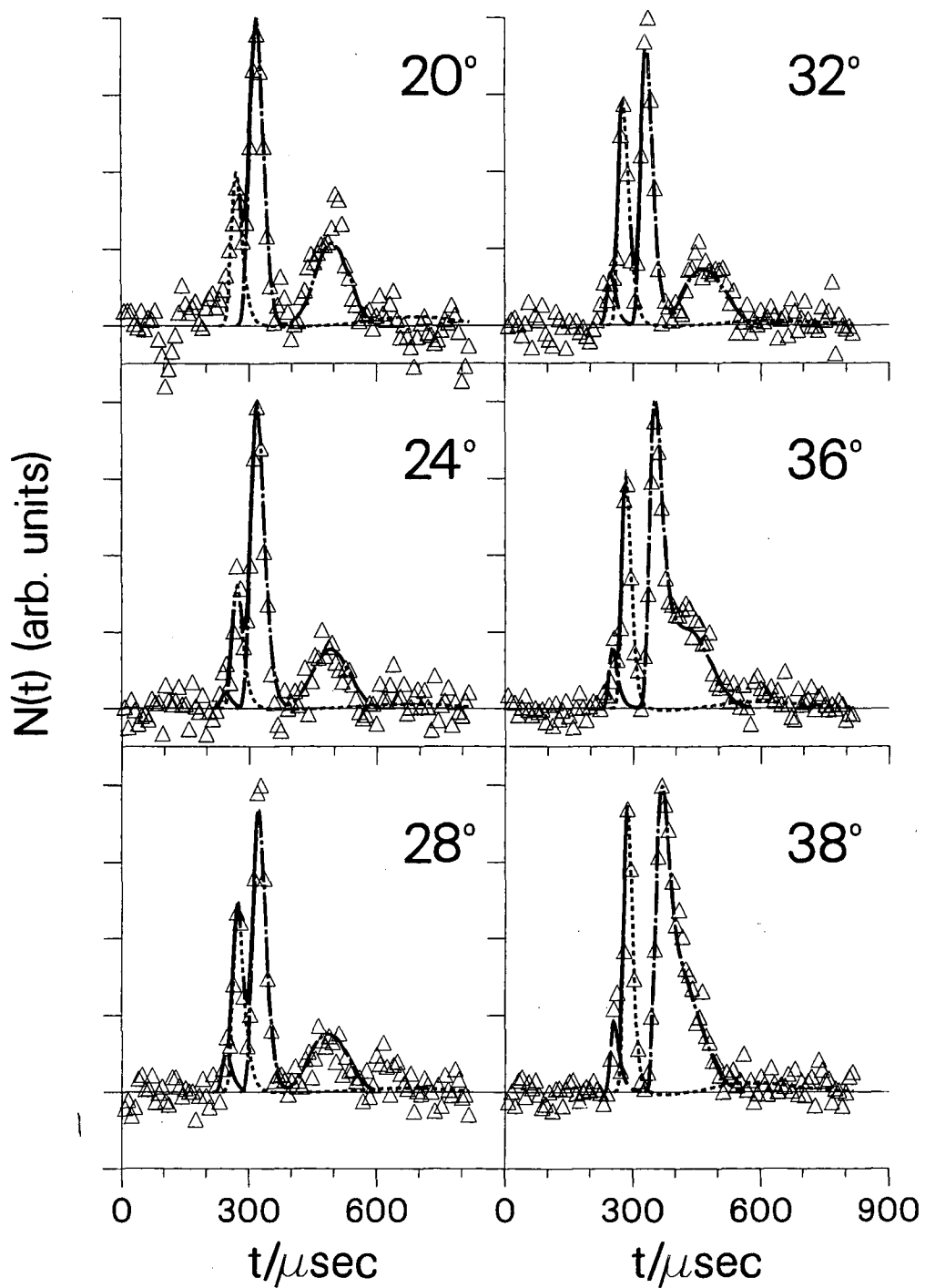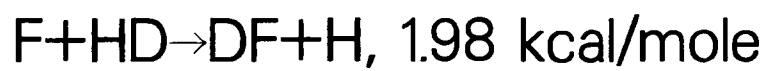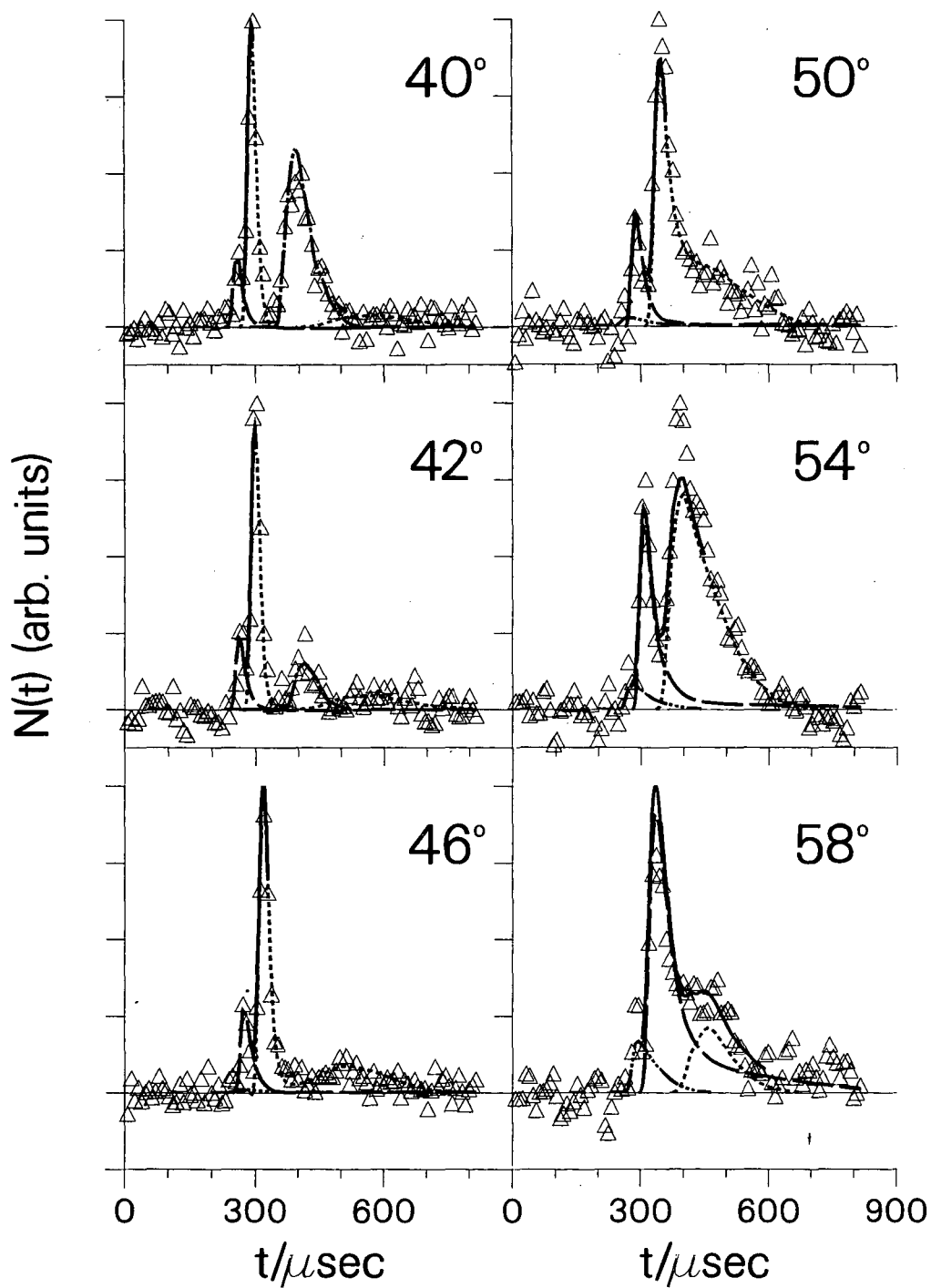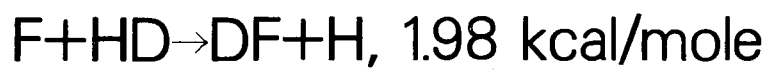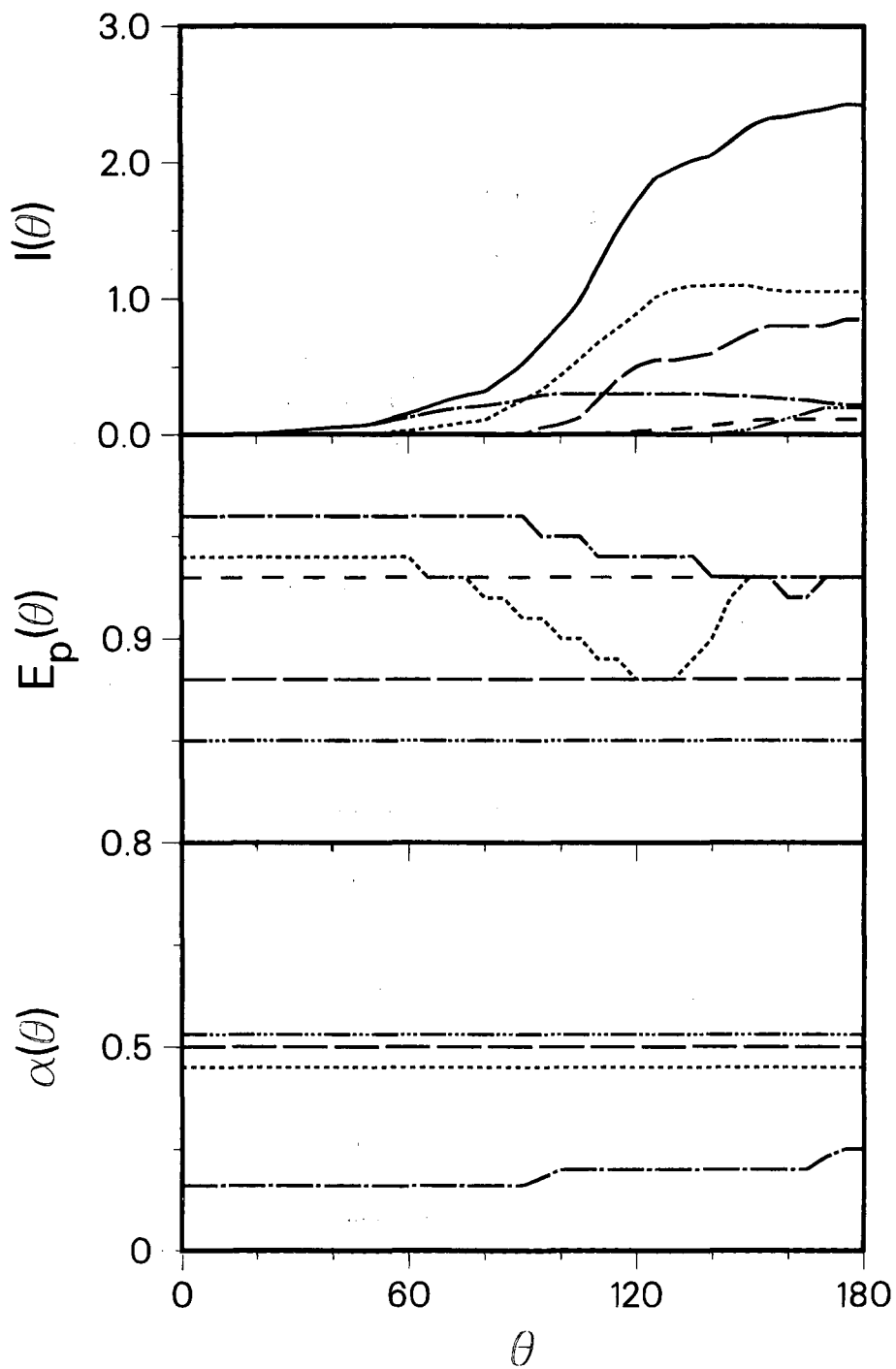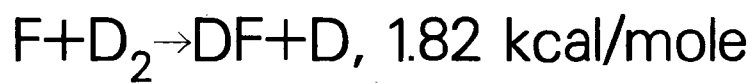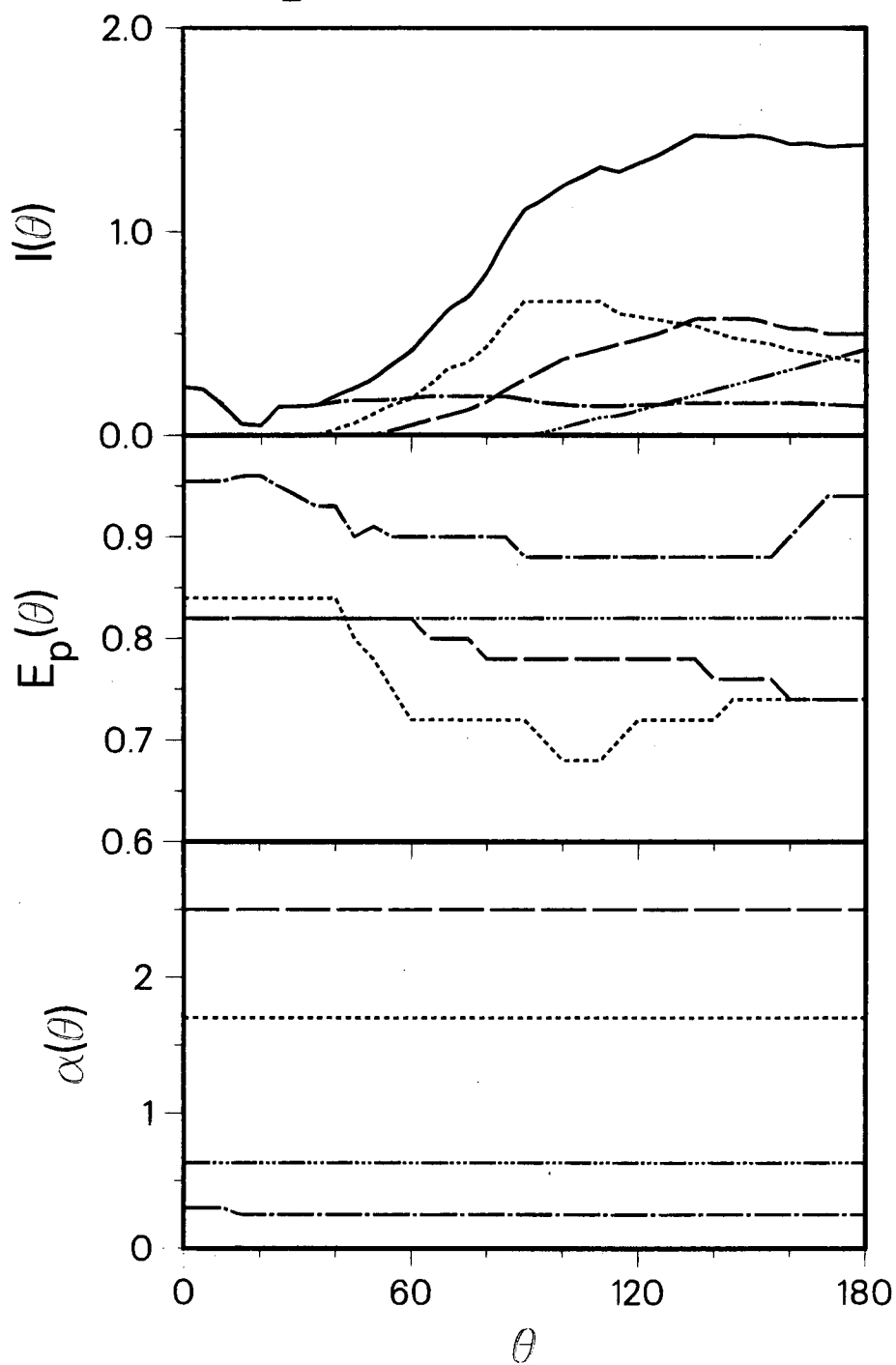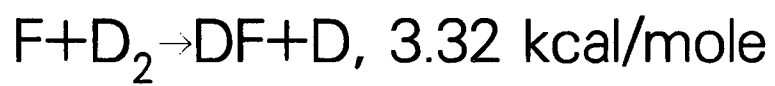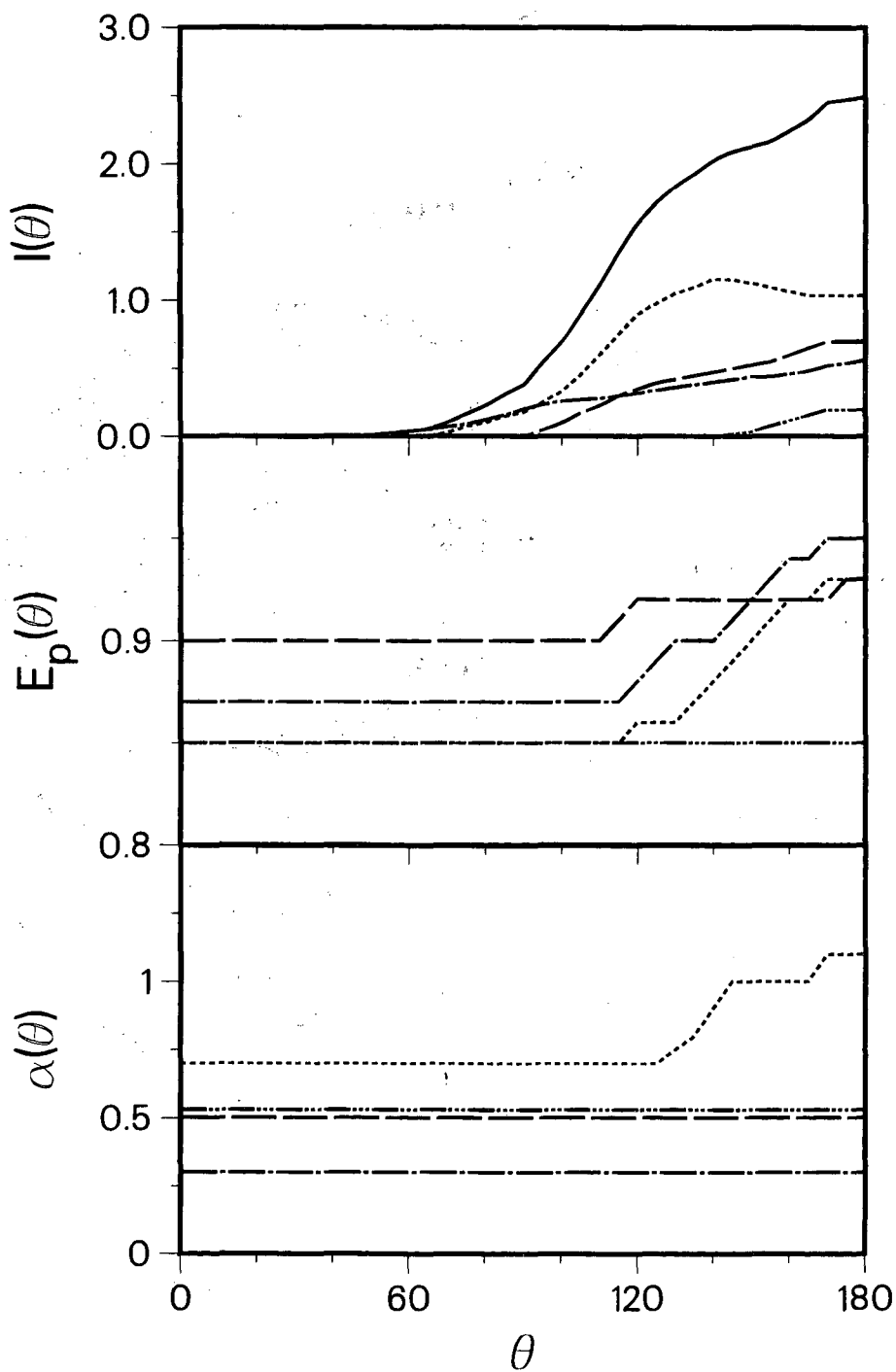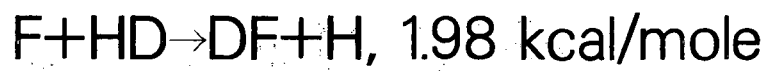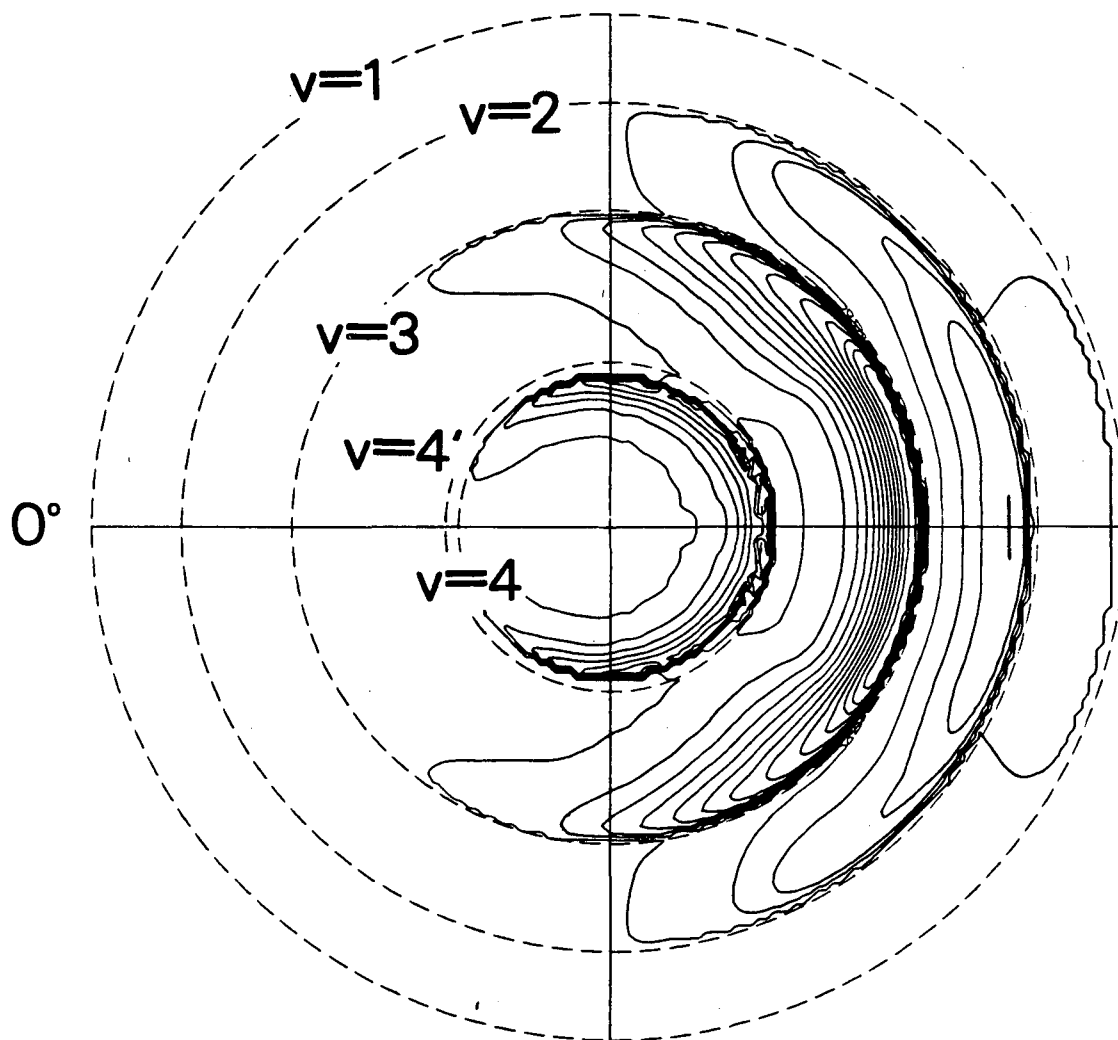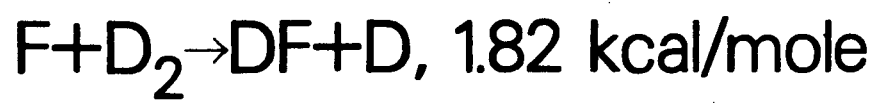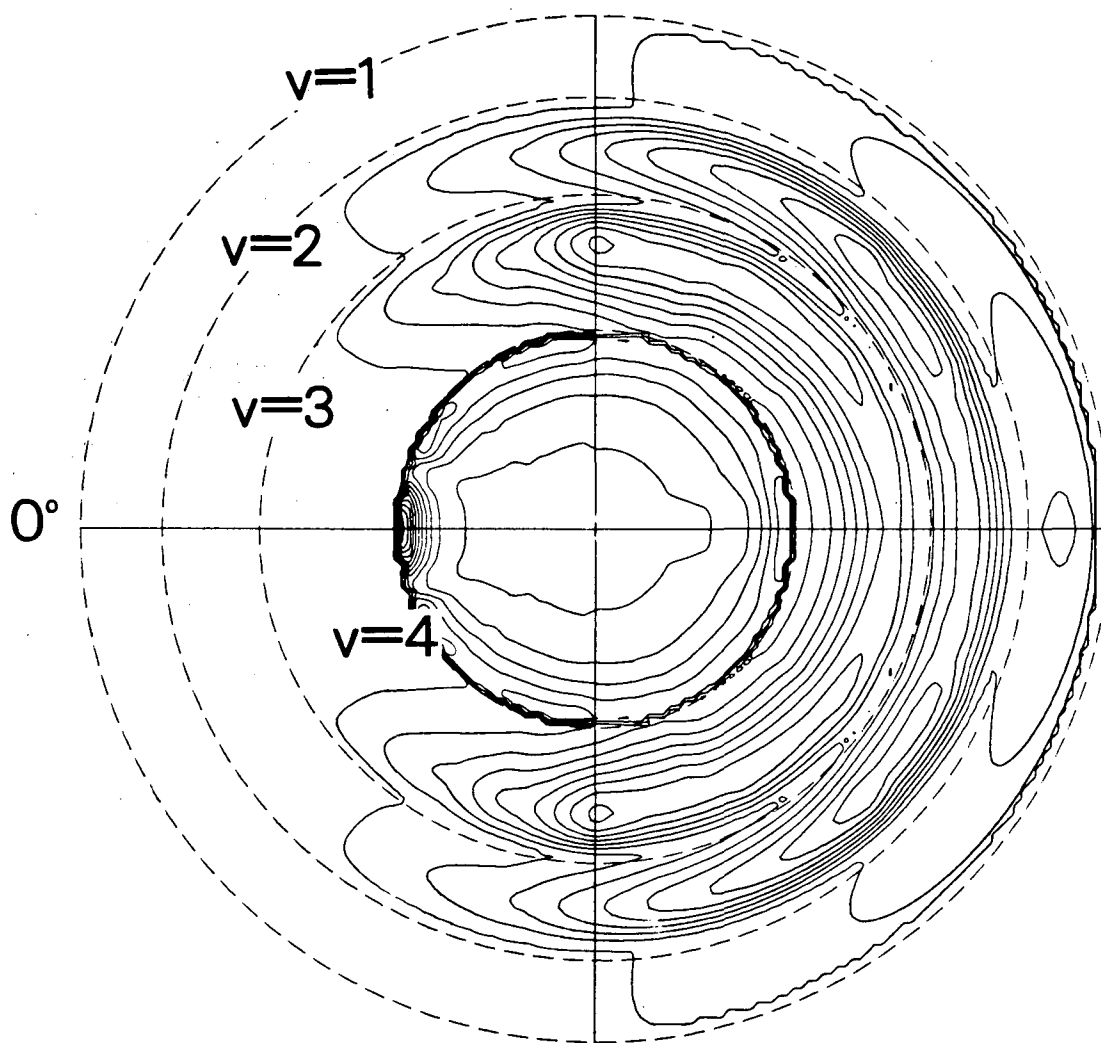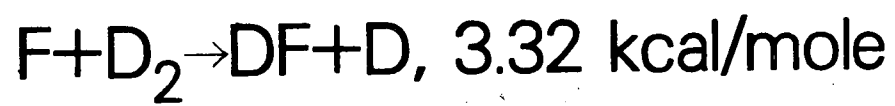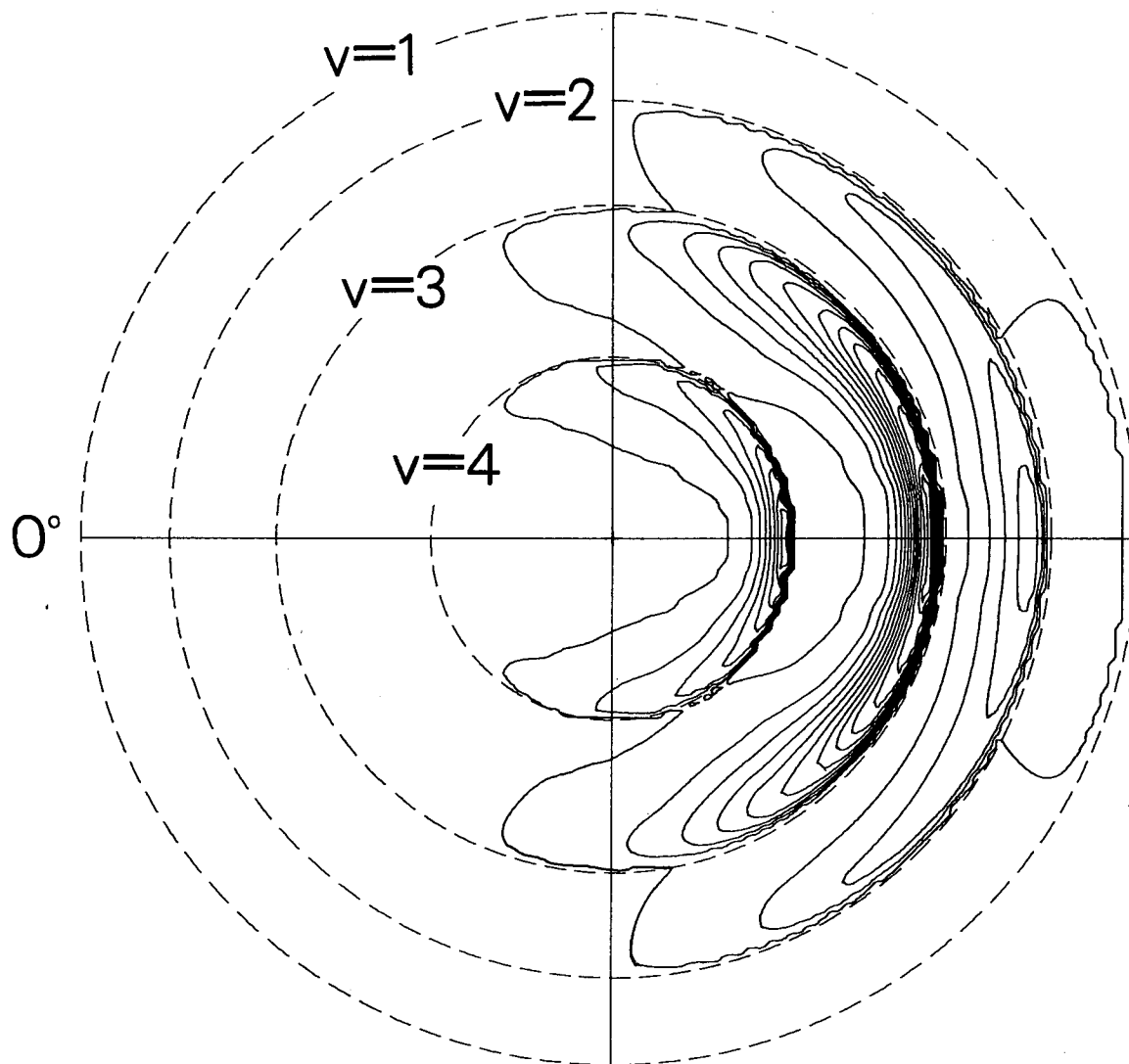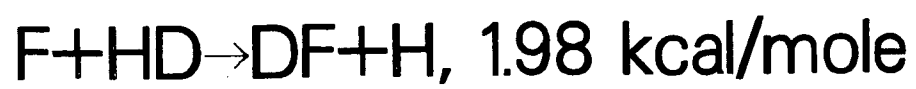
XBL 841-108

Fig. 16

Relative Cross Sections for F+D₂
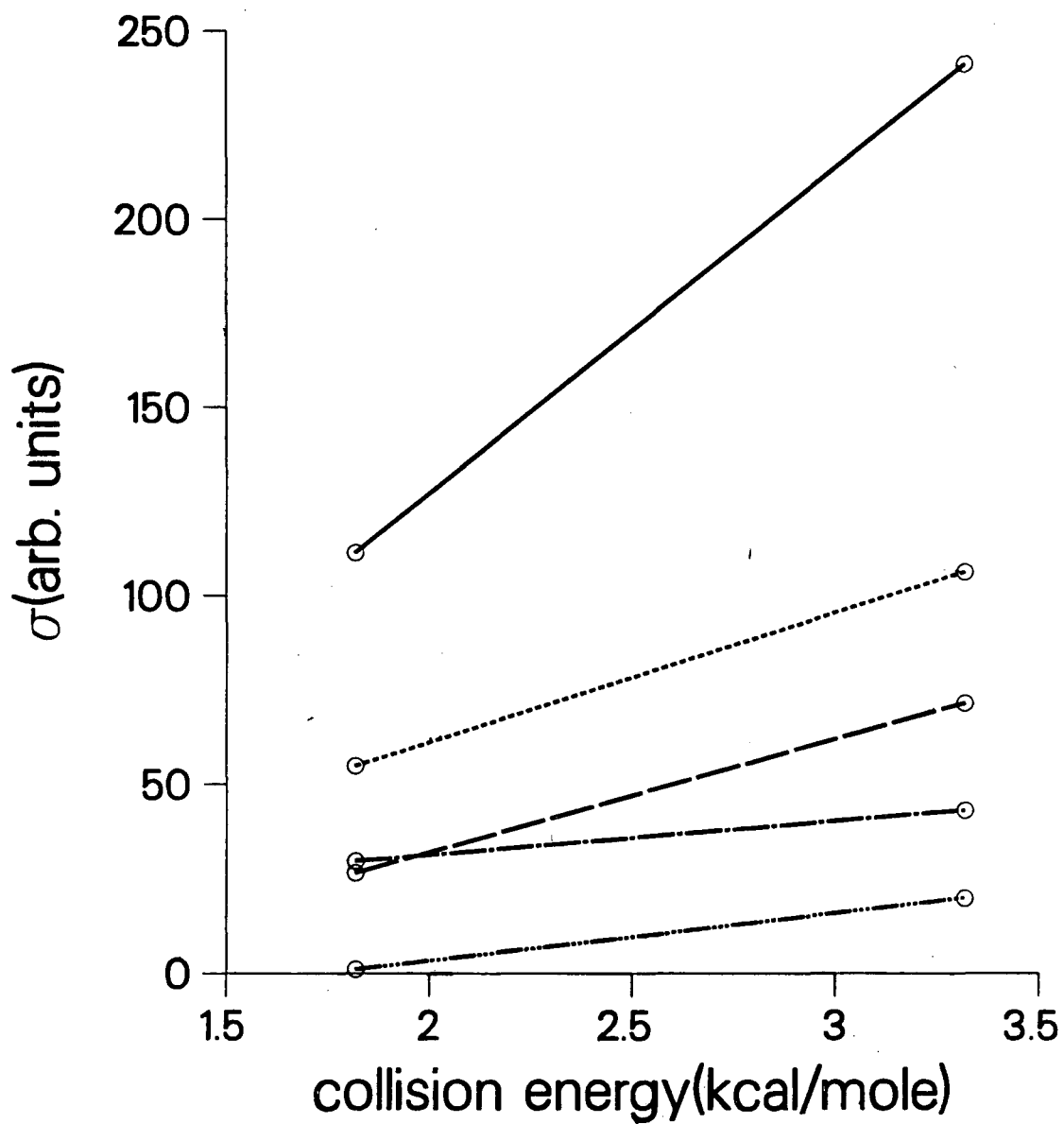
XBL 841-133

Fig. 17

Normalized Cross Sections for F+D$_2$

XBL 841-134

Fig. 18